

FINAL PUBLISHABLE JRP REPORT

JRP-Contract number	NEW03	
JRP short name	Nano ChOp	
JRP full title	Chemical and optical characterisation of nanomaterials in biological systems	
Version numbers of latest contracted Annex Ia and Annex Ib against which the assessment will be made	Annex Ia:	V1.3
	Annex Ib:	V1.1
Period covered (dates)	From 01 June 2012	To 31 May 2015
JRP-Coordinator		
Name, title, organisation	Dr Heidi Goenaga-Infante, LGC	
Tel:	+44 (0) 208 943 7000	
Email:	Heidi.Goenaga-Infante@LGCGroup.com	
JRP website address	http://nanochop.lgcgroup.com/	
Other JRP-Partners		
Short name, country	BAM, Germany	
	JRC, EU	
	NPL, UK	
	PTB, Germany	
REG-Researcher (associated Home Organisation)		
Researcher name, title (Home organisation Short name, country)	Zoltan Varga RCNS HAS, Hungary	Start date: 01 October 2013 Duration: 18 months
Researcher name, title (Home organisation Short name, country)	Eric Pitkeathly Heriot-Watt University, UK	Start date: 01 January 2013 Duration: 19 months
Researcher name, title (Home organisation Short name, country)	Christian Schmidtke UHAM, Germany	Start date: 01 November 2013 Duration: 12 months

Report Status: PU Public



RMG-Researcher
(associated Home Organisation)

Researcher name, title
(Home organisation Short
name, country)

Marcell Palmai
RCNS HAS, Hungary

Start date: 01 October
2013
Duration: 6 months



TABLE OF CONTENTS

1	Executive Summary	4
2	Project context, rationale and objectives	5
3	Research results	6
3.1	Objective 1: Production of a series of reference nanomaterials and characterisation of a suitable cell-based model(s) as a test system(s) for the interaction of nanomaterials with biological systems.....	6
3.2	Objective 2: Validation of a range of physical and chemical techniques for measuring the size and chemical composition of nanomaterials in a serum based biological system.....	12
3.3	Objective 3: Development of methods for the simultaneous characterisation of physical and chemical composition of nanomaterials in cell based biological systems.....	21
3.4	Objective 4: Development of traceable methods for the characterisation of 'bulk' optical properties of fluorescent nanomaterials, in particular quantum yield, absorption coefficient and corrected emission spectra.	27
3.5	Objective 5: Development of measurement techniques for biotechnology using fluorescent nanomaterials.	33
4	Actual and potential impact	37
5	Website address and contact details	38
6	List of publications.....	38

1 Executive Summary

Introduction

Nanomaterials are being used widely, and by an ever growing number of European industries to develop the next generation of high-performance products. However, the properties of nanomaterials are not always well understood, and there are concerns about their potential toxicity. This project developed reference nanomaterials and measurement techniques to describe their chemical, physical and optical properties in biological systems. These materials and techniques are being used to better understand the properties of nanomaterials to assess their health risks, but also to support the effective use of nanomaterials in a wider range of European industries and products.

The Problem

Nanomaterials are products that include structures smaller than 100 nanometres in length. Their small size, large surface area, and their quantum effects give them with a range of desirable properties such as increased strength, high elasticity, electrical conductivity, or radiation resistance. These properties are being used to develop the next generation of materials and products, and nanomaterials are used in an increasingly broad range of industries, including electronics, healthcare, cosmetics and clothing. However, although the properties of nanomaterials are attractive, they are not always well understood, and there are concerns about their potential toxic effects. To ensure the future competitive success of the wide range of European industries that use nanomaterials and, to understand their effects on health, traceable methods that measure accurately and generate comparable results for the properties of nanomaterials in biological systems are urgently needed. These will be invaluable to safety and risk assessments.

The Solution

In response to this problem, the project set out to develop and validate methods for the physical, chemical and optical characterisation of nanomaterials in relevant biological matrices (e.g. cell media). To achieve this, a range of reference nanomaterials and cell-based models were developed and made available. These were used to develop nanomaterial-measurement methods for properties including chemical composition, size, size-distribution, surface charge, agglomeration of silica-based nanomaterials and, optical properties of fluorescent nanomaterials in either serum-based system and/or attached to antibodies in biotechnology procedures. Methods and supporting materials to describe nanomaterial properties in biological media relevant to nanotoxicity studies are now available for the first time.

Impact

The project's outputs have already been disseminated extensively and shared with industry. They have been used to improve products and services for instrument manufactures and nanomaterial producers. The project has also had significant impact on standards for assessing nanoparticle properties and safety. Insights developed from the production of reference nanomaterials and relevant guidance on their in house preparation and characterisation have been shared with National Measurement Institutes (NMIs) and reference material producers.

In terms of future and wider impact, the reference nanomaterials and the measurement techniques developed by this project are the first of their kind, and will lead to a better understanding of the properties of current and future nanomaterials. They will also play a key role in ensuring the safe use of nanomaterials; for example the results will be used by nano-biotechnology and nano-medicine organisations to validate their protocols, and to perform toxicology studies and risk assessments. Further to this, regulatory bodies and legislators will benefit from a clearer understanding of the effects of nanomaterials on health, and will have a foundation upon which they can develop policies and guidelines. The important first step made by this project in the understanding of the properties of antibody-bound nanomaterials has laid the foundations for the increased use of nanomaterials in medicine and healthcare.

2 Project context, rationale and objectives

Context

Nanomaterials are products that include structures smaller than 100 nanometres in length. Their small size, large surface area, and their quantum effects give them with a range of desirable properties such as increased strength, high elasticity, electrical conductivity, or radiation resistance. These properties are being used to develop the next generation of materials and products, and nanomaterials are used in an increasingly broad range of industries, including electronics, healthcare, cosmetics and clothing. It is estimated that nanomaterials are used in over 1300 products in a global market currently worth €9.6 billion*. However, although the properties of nanomaterials are attractive, they are not always well understood, and there are concerns about their potential toxic effects. To ensure the future competitive success of the wide range of European industries that use nanomaterials, methods are needed to accurately measure their properties in order to understand their effects on health.

The techniques developed need to be traceable to agreed reference systems, to guarantee the accuracy and repeatability of their results, but before this project there were no established reference nanomaterials to ensure comparability of toxicity studies and materials testing. Nanomaterials are also typically tested in non-biological media, but when nanomaterials interact with biological systems their properties can change significantly. Before this project there were no robust methods to describe nanomaterial properties in biological media such as cell cultures. New techniques were urgently needed to measure the physical, chemical and optical properties of nanomaterials in biological systems for safety and risk assessments.

*McWilliams G A A 2010 BCC Market Research Reports (NAN031D) p 1–276

Objectives

The following five objectives were identified to achieve the overall goal of developing methods to measure the properties of nanomaterials in biological systems. Objective 1 developed a range of reference nanomaterials, and cell-based models that represent biological systems. These reference materials and biological systems were then used to develop nanomaterial measurement methods, including: size and chemical properties in a serum-based biological system (objective 2); real-time measurement of physical and chemical properties in a cell-based biological system (objective 3); optical properties of fluorescent nanomaterials in a serum-based system (objective 4); and fluorescent properties of nanomaterials attached to antibodies in biotechnology procedures (objective 5).

1. To produce a series of nanomaterials (for example, inorganic oxides and quantum dots) that are characterised in their native form for size, surface charge and fluorescence. To characterise a suitable cell-based model(s) for its application as a test system(s) for the interaction of nanomaterials with biological systems.
2. To validate the use of a range of physical and chemical techniques for measuring the size and chemical composition of nanomaterials in a serum based biological system.
3. To develop methods for the simultaneous characterisation of physical and chemical composition of nanomaterials in cell based biological systems.
4. To develop traceable methods for the characterisation of 'bulk' optical properties of fluorescent nanomaterials, in particular quantum yield, absorption coefficient and corrected emission spectra.
5. To develop measurement techniques for biotechnology using fluorescent nanomaterials.

3 Research results

3.1 Objective 1: Production of a series of reference nanomaterials and characterisation of a suitable cell-based model(s) as a test system(s) for the interaction of nanomaterials with biological systems.

The aim of this work was to develop a range of reference nanomaterials, and cell-based models that represent biological systems. Specifically to produce a series of nanomaterials (for example, inorganic oxides and quantum dots) that are characterised in their native form for size, surface charge and fluorescence. To characterise a suitable cell-based model(s) for its application as a test system(s) for the interaction of nanomaterials with biological systems.

With input from stakeholders (Izon, Nano KTN and NanoSight), the consortium agreed on the following materials to be developed:

Reference nanomaterials (RM)

- RM1: aminated silica
- RM2: titanium dioxide
- RM3: quantum dots

Fluorescent nanomaterials (FM)

- FM1-2: based on RM1
- FM3-4: based on polystyrene

To enable comparison of results of fluorescently labelled and non-labelled nanomaterials, the selected silica material would be provided in aminated form, ready for labelling with different fluorophores. A green emitting dye would be used to label RM1 to produce FM1 & FM2 and a red emitting dye would be used to stain polystyrene particles to produce FM3 & FM4.

The liver cell line HepG2 was selected as the cell model to expose the nanomaterials to and Foetal Bovine Serum (FBS) Gold as the biological matrix.

The following analytical techniques were used to compare the suspensions with the agreed target properties:

- Dynamic light scattering (DLS): equivalent spherical hydrodynamic diameters of nanomaterials based on the rate of their diffusion in the suspension due to Brownian motion
- Centrifugal liquid sedimentation (CLS): fractionates particles using sedimentation to provide values of the modal Stokes diameter, (d_{CLS})
- Small-angle X-ray scattering (SAXS): for particles with a sufficiently narrow size distribution, periodic intensity oscillations are observed, the frequency of which can be related to the mean particle diameter, (d_{SAXS})
- Electrophoretic light scattering (ELS): measures zeta potential values of suspended nanomaterials, which are an indicator of the stability of electrostatic-based colloidal suspensions
- The microbiological load of the nanoparticle suspensions was examined using plating on nutrient agar

Selection and production of reference materials RM1-3

Reference Material 1 (RM1)

A suspension of aminated silica was sourced from a commercial supplier, diluted and filled in pre-scored amber glass ampoules. It was soon noticed that the material contained a viable microbiological load and the ampoules

were gamma-irradiated. Despite the successful gamma irradiation, this material was not progressed further because the effect of the visible flocs (particles clumped together) on the DLS data.

An alternative material (carboxylated colloidal silica) was sourced for the same commercial supplier but again, for reasons of impurity (flocs and bacterial contamination) preparation of this material was stopped.

A new aminated silica material was prepared by one of the project's Researcher Excellence Grants (REG) RCNS HAS. This material was prepared from Klebosol 30R50, a colloid of dense silica particles following an amination protocol developed previously. This material was further processed and ampouled by project partner JRC and distributed to all other project partners.

Reference Material 2 (RM2)

As it was not possible to obtain a well-dispersed and stable suspension of Titanium dioxide particles in the desired size range (near 20 nm) with a sufficiently low polydispersity, it was decided to exchange this material for plain (non-functionalised) colloidal silica.

The first material sourced from a commercial supplier again had issues with bacterial contamination and was not processed any further. Therefore, alternative plain colloidal silica was prepared from the same batch of Klebosol 30R50 used for RM1. This material was selected as the final RM2 material as it met the polydispersity criterion and was free from any relevant contamination. The material was diluted and ampouled by project partner JRC and distributed to all other project partners.

Reference Material 3 (RM3)

RM3 was prepared from an aqueous suspension of Cadmium selenide (CdSe)/ Cadmium sulphide (CdS)/ Zinc Sulphide (ZnS) quantum dots covered with a shell of Polyethylene glycol (PEG) molecules with amine end-functions. The base suspension was diluted with ultrapure water and filled into ampoules and sterilised by gamma irradiation. Bacterial contamination was remediated with the gamma irradiation, but the material was affected by agglomeration and contained larger particles that were visible in the ampoules. This made the material unsuitable to be conjugated to an antibody as required for use in an immuno-assay.

Status of the selected test nanomaterials

For the selected nanomaterials RM1 (aminated colloidal silica), RM2 (plain colloidal silica) and RM3 (quantum dots), their homogeneity and stability were studied in terms of average equivalent diameters and zeta potential. Stability of the nanomaterials was promoted by packing the suspensions in flame-sealed amber glass ampoules, argon flushed prior and/or after filling. The effects of time and temperature were also investigated in dedicated isochronous stability studies. The results of these homogeneity and stability tests determined the reference material status of the test materials; reference material (RM), reference test material (RTM) or test material.

Tables 1-3 summarise the main characteristics of the selected materials and indicates for each of the listed properties the corresponding status of the nanomaterial. The values in the tables are not provided with the metrological traceability statement and measurement uncertainty required to use them as certified values. The U_h and U_{ts} values indicate how much of the experimental variation observed by a user of the test materials can come from between-ampoule differences or from the time between different measurements.

Table 1 shows that the homogeneity and stability of RM1 was confirmed via DLS, CLS and SAXS measurements, and is an RM for measurements of these or related equivalent diameters, if it is properly stored (at 4 °C) for a period of maximum 36 months. It must be noted that the stability and homogeneity of the measured equivalent diameters improve when the methods are less sensitive to matter attached to or collected on the surface of the particles: the SAXS value is more stable than the CLS value, which is more stable than the DLS value. However, due to the slowly progressing change of DLS and ELS detected in the stability studies, RM1 was not considered an RM or RTM for measurements of DLS and ELS.

Table 1		RM1 (aminated colloidal silica)		
General description	Aminated silica nanomaterials, nominal mass fraction 2.5 g/kg			
Specific observations	Free of active bacterial contamination Particles visible to the naked eye have formed over time			
Instructions for use	Minimum sample intake 0.2 mL; store at 4 °C; avoid freezing; close opened ampoule with paraffin film; use within 5 days after opening.			
Equivalent diameters	Measured value	u_h	U_{its} (36 months)	status
$d_{DLS,NNLS,i}$	89.9 nm	0.3 %	(5.9 % when stored at 18 °C)	Test material
$d_{CLS,i}$	88.4 nm	0.2 %	(1.3 % when stored at 18 °C)	RM
$d_{SAXS,nb}$	(81.8 ± 0.8) nm	0.02 %	(0.1 % when stored at 18 °C)	RM
Other measured properties				
ζ_{ELS}	9.7 mV	0.8 mV	(2.8 mV when stored at 18 °C)	Test material
pH	3	-	-	Test material

Table 2 shows that the homogeneity and stability of RM2 was confirmed via DLS and CLS measurements. Therefore RM2 is an RM for these particle size analysis techniques. The same RM status was also assigned for the SAXS method. This is possible because the DLS and CLS measurements are sensitive to more aspects that have an effect on the stability of the silica nanoparticle sizes than SAXS, which is a more robust method, only sensitive to changes of the solid nanoparticle core itself. The combined DLS and CLS data guarantee the stability and homogeneity of the material in terms of dSAXS for this type of colloidal silica. Based on its excellent stability in terms of particle size, and on measurements by ELS, RM2 was also considered a RTM for ELS, the only additional requirement being that ELS is measured on the day of opening the ampoule.

Table 2	RM2 (plain colloidal silica)			
General description	silica nanomaterials, nominal mass fraction 2.5 g/kg			
Specific observations	Free of active bacterial contamination			
Instructions for use	Remove cloud formation by repeated inversion; minimum sample intake 0.3 mL; store at room temperature; avoid freezing; close opened ampoule with paraffin film; use within 10 days after opening (or on day of opening for measurement of ζ_{ELS}).			
Equivalent diameters	Measured value	u_h	U_{ITS} (36 months)	status
$d_{DLS,cum}$	90 nm	-	1.1 %	RM
$d_{DLS,NNLS,i}$	94 nm	1.0 %	2 %	RM
$d_{CLS,i}$	87 nm	0.5 %	2 %	RM
$d_{SAXS,nb}$	(81.1 ± 0.8) nm	-	-	RM
Other measured properties				
ζ_{ELS}	-48 mV	1.8 mV	-	RTM
pH	8.4	-	-	Test material
Effective particle density	2.0 g/cm ³	-	-	Test material

Table 3 indicates the status of RM3. The presence of large fibre-like particles prevented it from being used as a reliable RM, and as such the long-term stability of the material was not quantitatively evaluated.

Table 3	RM3 (quantum dot)			
General description	Aminated CdSe/CdS/ZnS QDs, aqueous, nominal concentration 1 μ mol/L.			
Specific observations	Sterilised by gamma irradiation (6.4 kGy), Containing a fraction of fibre-like particles visible to the naked eye			
Instructions for use	Minimum sample intake 0.1 mL; store at room temperature; avoid freezing; use contents of an ampoule on the day of opening			
Equivalent diameters	Measured value	u_h	U_{ITS} (36 months)	status
$d_{DLS,cum}$	103 nm	2.2 %	-	Test material
$d_{DLS,NNLS,nb}$	31 nm	7 %	-	Test material
Other measured properties				
ζ_{ELS}	-1.4 mV	0.6 mV	-	Test material
pH	5	-	-	Test material
Absorption maximum (first excitonic peak)	598 nm	-	-	Test material
Emission maximum (FWHM)	612 nm (< 30 nm)	-	-	Test material
Photoluminescence quantum yield	0.14	-	-	Test material

The project demonstrated that SAXS was an excellent method to assess the width of the peak in a monomodal nanoparticle size distribution and the homogeneity and stability of the average diameter of the solid core of silica nanomaterials. Other techniques provided a fuller picture of the presence and stability of other particulate fractions. For example DLS is very effective in detecting small numbers of large particles, also if they are of low density (flocs, loose agglomerates) but visual inspection remains essential to detect foaming and flocculation. CLS, being a fractionation technique, provided useful information on the presence of smaller peaks, e.g. from small aggregates of the main nanoparticle population.

Selection and production of fluorescent nanomaterials FM1-4

Project partner BAM labelled RM1 (aminated silica particles) with reactive (N-Hydroxysuccinimide (NHS) ester activated) fluorescent dyes DY556-NHS and DY557-NHS to produce the fluorescent silica nanomaterials FM1 and FM2 respectively. Samples were distributed to all project partners.

Commercial polystyrene particles (100 nm in size), surface functionalised with either carboxylic acid groups or amino groups, were stained with the fluorescent dye DY680-COOH to produce the fluorescent silica nanomaterials FM3 (carboxylated particles) and FM4 (aminated particles), respectively. Samples were then distributed by BAM to all other project partners.

Fluorescent dyes were chosen with regard to their emission wavelength (to fit the detection wavelengths of the instruments to be used within the project), their reactive groups (NHS ester function for RM1 labelling), and their solubility in the reaction media (aqueous media for RM1 labelling to produce FM1/2, Dimethylformamide (DMF) for Ponceau S (PS) staining to produce FM3/4).

Sourcing and characterisation of cell systems

LGC obtained the HepG2 cell model selected from an external supplier and created a cryopreserved master cell bank. A protocol for the optimised seeding density was developed and validated.

A common protocol for dispersion of nanomaterials RM1, RM2, RM3, FM1 and FM2 in aqueous and biological (cell culture) media was developed at LGC and circulated to project partners. Protocols for the administration of RM1, RM2, RM3, FM1 and FM2 materials into the HepG2 model were also developed.

In order to understand how nanomaterials penetrate and localise in cells, the uptake of fluorescently labelled nanomaterials FM1 and FM2 (based on the aminated colloidal silica 'RM1') was determined by confocal microscopy at LGC, with further verification by Transmission Electron Microscopy (TEM). Results showed that the particles were internalised by the HepG2 cells and confined in intracellular organelles. The presence of silica particles inside the cells was correlated with an increased production of reactive oxygen species (ROS) and pro-inflammatory cytokines (markers of cell stress). RM1 and RM2 exhibited dose-response properties, strongly indicative of a biological effect on the HepG2 cells.

LGC also generated samples of cell lysates following treatment of the cell model with RM1 and RM2 and distributed to project partner PTB for simultaneous physical and chemical characterisation by SAXS and X-ray fluorescence (XRF).

Conclusions

Reference nanomaterials and cell-based test systems were required as a first step, from which techniques could then be developed to measure the properties of the nanomaterials in the test biological systems. Manufactured silica nanoparticles were the focus of this research as they are commonly used as food additives. However, nanomaterials with ideal properties (e.g. spherical, monodisperse) were developed, rather than the typical nanomaterials used in everyday life, as this project represents the first step in addressing the measurement challenges of nanoparticle properties in biological systems.

A series of nanomaterials were produced in suspension, including plain colloidal silica and NH₃-modified colloidal silica (i.e. inorganic oxides for physical and chemical characterisation), fluorescently labelled inorganic oxides (e.g. fluorescently labelled silica for monitoring within biological cells), and quantum dots (for optical characterisation).

Homogeneity and stability studies were completed for each of the nanomaterials in suspension, and material information sheets were produced for each summarising their main characteristics. Protocols for dispersion of the nanomaterials in water, buffered aqueous solutions (e.g. Tris-HCl buffer solutions) and biologically relevant media were developed. The liver cell line HepG2 was selected as a suitable cell model to be exposed to the nanoparticles to characterise their properties in biological systems, and toxicity studies were undertaken. These showed that whilst quantum dots had no significant toxic effect, plain colloidal silica nanoparticles exhibited dose-response toxic properties, strongly indicative of a biological effect on the liver cells.

The project successfully achieved the objective as a series of reference nanomaterials were produced, appropriate cell-based test systems were identified, allowing the reference nanoparticles to be characterised in both their native form as well as within biological systems. The reference nanomaterials were then used by project partners for method development, validation and instrument calibration to deliver objectives 2-5.

3.2 Objective 2: Validation of a range of physical and chemical techniques for measuring the size and chemical composition of nanomaterials in a serum based biological system.

The aim of this work was to use the reference materials from objective 1 to develop nanomaterial measurement methods, including: size and chemical properties in a serum-based biological system. More specifically to validate the use of a range of physical and chemical techniques for measuring the size and chemical composition of nanomaterials in a serum based biological system.

Influence of biological media on size measurements

Size is the defining property of nanomaterials. It can be determined with high accuracy by selected techniques that can produce SI-traceable results without the use of certified reference materials (CRMs), for nanomaterials dispersed in plain aqueous media. However, the determination of the size of nanomaterials in complex biological media is challenging not only because the commonly used sizing techniques are less accurate in multi-component systems, but also because of the possible interactions between the nanomaterials and the constituents of the biological matrix. Further to this, the protein corona, which forms on the surface of nanomaterial particles when in contact with biological material, can influence the measured size in two ways:

1. measurement techniques which are sensible to the size including the corona will find an increase in size due to the additional layer on the surface,
2. the biological matrix can also indirectly influence the measured size by disturbing the measurement technique itself, which is usually adjusted to measurements in pure solvents only.

The particle size and particle size distribution of RM1 (aminated colloidal silica) and RM2 (plain colloidal silica) nanomaterials were measured by DLS, CLS, SAXS and PTA after dispersion in i) purified water, ii) Tris-HCl buffer at a physiological pH and iii) in cell culture medium containing 10% bovine serum (FBS), all following the protocol developed by project partner LGC. Samples were measured by all methods immediately after dispersion and after incubation at room temperature for 24 h. The measurements were complemented by uncertainty analyses, in order to evaluate the influence of the dispersion medium on the resulting size values.

The results are summarised in **Figure 1**. The modal values for the suspensions in water and Tris buffer are displayed in number- and volume-weight in (a) and (b), respectively. In number weighting, PTA, CLS and SAXS agreed within their expanded ($k=2$) uncertainties, whereas DLS gave consistently lower results. Volume-weighted particle-size distribution (PSD) for PTA was not available, but the other three methods (DLS, CLS, SAXS) agreed on the volume-weighted data, with the exception of RM2 in Tris-HCl buffer, where DLS reported a slightly smaller value.

As an example for the behaviour of the sizing methods in the biological medium, the PSDs for RM1 immediately after dispersion are shown in number- and volume-weight in **Figure 1e** and **Figure 1f**, respectively. Both SAXS and CLS showed a sharp maximum around 80 nm and a broader peak below 50 nm. The CLS volume-weighted distribution contained an additional broader peak between 100 nm and 200 nm, with distinct peaks at 100 nm and 110 nm of the same width approximately as the primary peak, but smaller height. The DLS results were inconsistent and differed significantly from the other methods. Even for repeated measurements on a single aliquot, the obtained PSD differed vastly, as illustrated by the green lines in **Figure 1f**. Several reasons are likely to be responsible for this; DLS as an ensemble technique is very sensitive to large particles such as agglomerates, thus when their presence is in minute amounts, the distribution can be significantly weighted towards these agglomerates. Therefore, DLS was not considered in further comparisons.

Although PTA is based on the detection of Brownian motion like DLS, the quality of PTA measurements did not deteriorate when applied to the dispersions of the reference nanomaterials in biological medium. However, these results could only be obtained using a newer NTA software version (3.0), as older algorithms were affected by measurements in cell culture medium. Therefore, only number-weighted PSDs were directly obtained using this method.

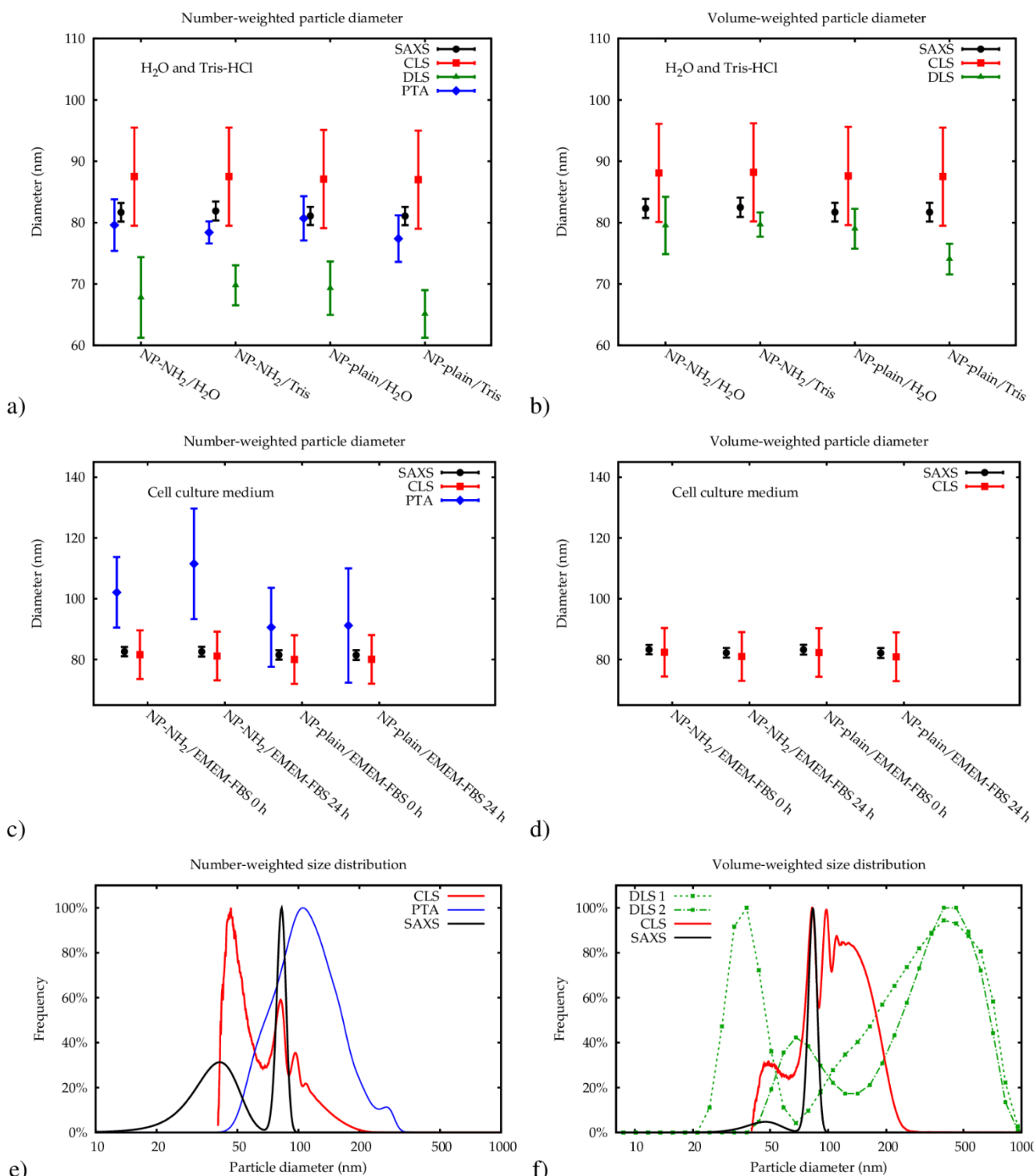


Figure 1: Comparison of size measurement results. The modal diameters determined for the dilution in water and Tris-HCl, directly after dispersion are shown in (a) for number-weighted PSDs and in (b) for volume-weighted PSDs. The error bars denote expanded ($k=2$) uncertainties. The modal diameters measured in cell culture medium are displayed in (c) and (d), respectively. Here, the error bars for PTA and CLS do not include the additional unknown uncertainty contribution for measurements in complex media. Representative PSDs for the dispersion of RM1 in cell culture medium are shown in (e) and (f). The two results for DLS obtained from two consecutive runs of the same aliquot (dashed and dash-dotted green line) illustrate the repeatability issues of DLS in complex media.

The modal diameters obtained for RM1 and RM2 on both points in time are compared in **Figure 1e** and **Figure 1f**. The size of the core of the primary particle fraction was best resolved in the SAXS measurements, which show almost no indication of other fractions (agglomerates, aggregates, smaller particles). The SAXS technique was not affected by or sensitive to the functional amino-groups on RM1 and was only minimally, but measurably, affected by the dynamic development of a protein corona on the surface of the RM1 and RM2 particles. Consequently, all SAXS measurements agreed within the standard uncertainties.

The CLS data allowed the resolution of different fractions like primary nanoparticles and different levels of agglomeration/aggregation. However, the interpretation of the measured size values was not straightforward, due to the opposite effects on sedimentation time of the developing protein corona. Nevertheless, the size obtained for the primary particle fraction was consistent with the SAXS results within the expanded uncertainties.

Influence of fluorescent staining on size measurements

Fluorescent nanomaterials such as dye-stained polymer particles, dye-labelled silica-particles and semiconductor quantum dots are increasingly used as reporters in various bioanalytical applications for in vivo and in vitro spectroscopy and imaging. Therefore, the influence of fluorescence on nanoparticle size measurements using DLS and SAXS was investigated here. Whereas SAXS depends on the scattering of X-rays based upon the electron density of the particles, and should therefore be independent of any fluorescence signals, DLS relies on light scattering and may thus be affected by the absorption and emission of labelled dyes or self-luminescent nanomaterials. Depending on the optical properties and the wavelength of the laser used for the DLS measurements, absorption can result in a partial loss of the coherent incident light and the subsequently emitted non-coherent fluorescence may also affect the measured signal. Although comparisons between DLS and SAXS size measurements in standard settings are available for different particle systems such as micelles, proteins, and polymers, prior to the NEW03 project there were no systematic investigation on the influence of fluorescence on these particle size measurement techniques.

To address this, two series of 100 nm-sized polymer nanomaterials stained with different concentrations of the fluorescent dyes DY555 (green) and DY680 (red) were prepared by the project, absorbing/emitting at around 560 nm/590 nm and 695 nm/715 nm, respectively. These dyes were specifically selected to match the laser wavelengths of the used instruments. The DLS experiments were carried out in three different partners BAM, JRC and NPL using instruments equipped with either a red 633 nm He-Ne laser or a green 532 nm argon laser, such that the red laser only excites the red dye DY680, but not the green one, and vice versa.

The SAXS results are displayed in **Figure 2a**. As can be seen, within the stated standard uncertainties, no influence of the fluorescent dye was observed, as expected. Due to the fact that the nanoparticles were all prepared from the same precursor material and treated in a very similar manner, these values can also be compared within the uncertainty given by the reproducibility of SAXS measurements. The reproducibility of SAXS measurements on these samples was previously determined by measuring the precursor material three times over a course of two years, with a variation of the resulting best fit diameter below 1 nm. Even within this reduced uncertainty all diameters of the dye loaded particles and the blank agreed. Therefore, it can be concluded that the particle diameter does not change by more than 1 nm due to the dye staining, and that the fluorescence had no significant effect on the SAXS measurements.

In contrast, a wavelength dependent effect of the fluorescence could be found in the raw correlation data recorded by DLS (**Figure 2b**). Here, the correlation coefficient at small correlation times decreased with increasing staining concentration, when the dye was excited by the laser (top left and right bottom graph in **Figure 2b**), whereas no effect was observed if there is a mismatch between dye absorption and laser wavelength (top right and bottom left graph).

Nanoparticle size determination with DLS was not affected by dye-staining when the fluorophore concentration was low. **Figure 3** shows the Z-average values of the particle diameters obtained from three different instruments at two partners BAM and NPL on the same samples. No significant change or trend was observed between different dyes or compared to the blank. The measured sizes and size distributions (not shown here) were also independent of the instrument and/or the operator (similar results obtained in all laboratories), the dye absorption wavelength (similar results for DY555- and DY680-stained particles) or the dye staining

concentration (similar results for all particles of a staining series with dye concentrations ranging from 0 to 1 mM), if the same type of instrument was used. Moreover, **Figure 3** shows that no significant size differences were detected between and within the two different particle series at different laser wavelengths.

These results demonstrate the need to recommend the use of a bandpass filter in front of the DLS detector to remove fluorescence photons for the reliable size measurement of strongly emitting particles. The loss in scattering photons by strong absorption of the incident laser light can be best compensated for by more repetitions as an increase in particle concentration may favour particle aggregation.

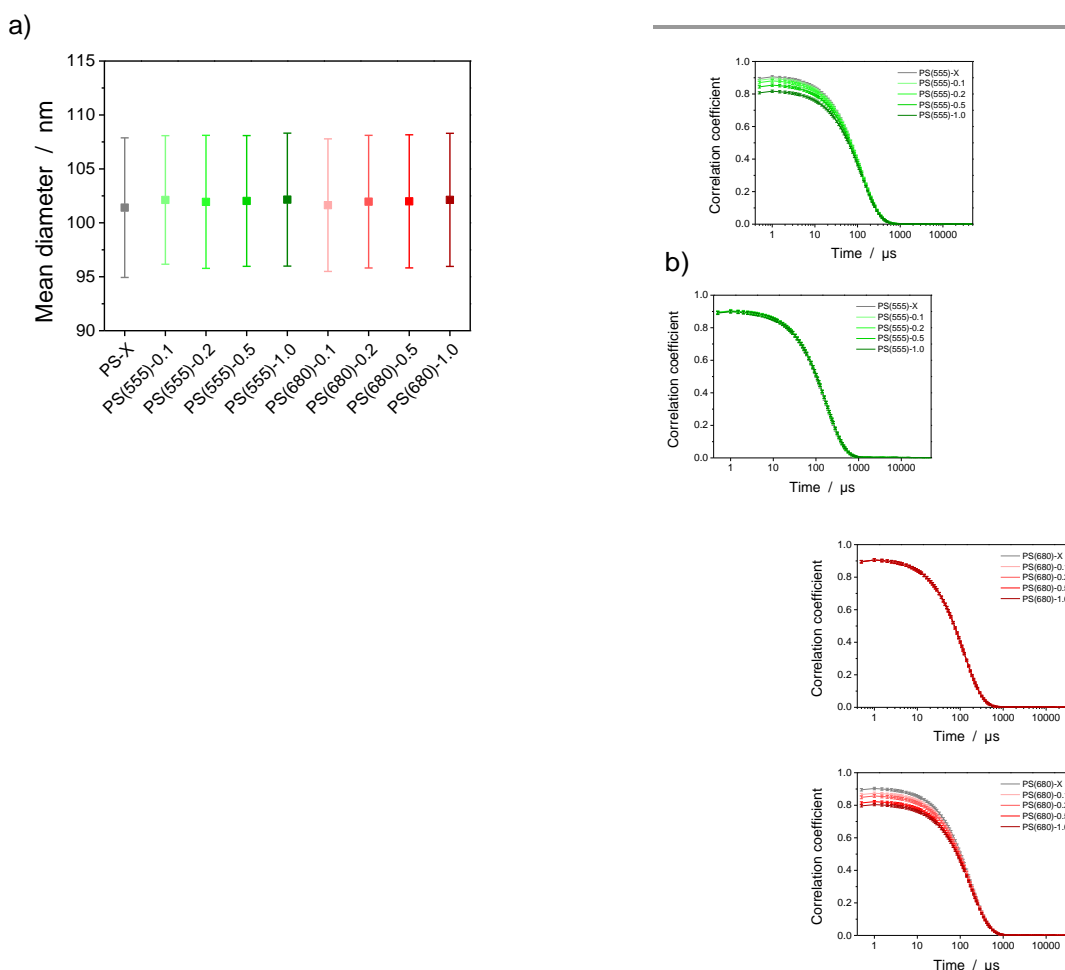


Figure 2: a) Size measurement results for the dye-stained nanoparticle samples as measured with SAXS. The coloured squares and bars represent the mean diameters and standard uncertainties, respectively. **b) Correlation coefficients as measured with DLS for the DY555-stained (top) and DY680-stained (bottom) PS particles at the “green” Zetasizer with 532 nm laser (left) and at the “red” Zetasizer with 633 nm laser (right).**

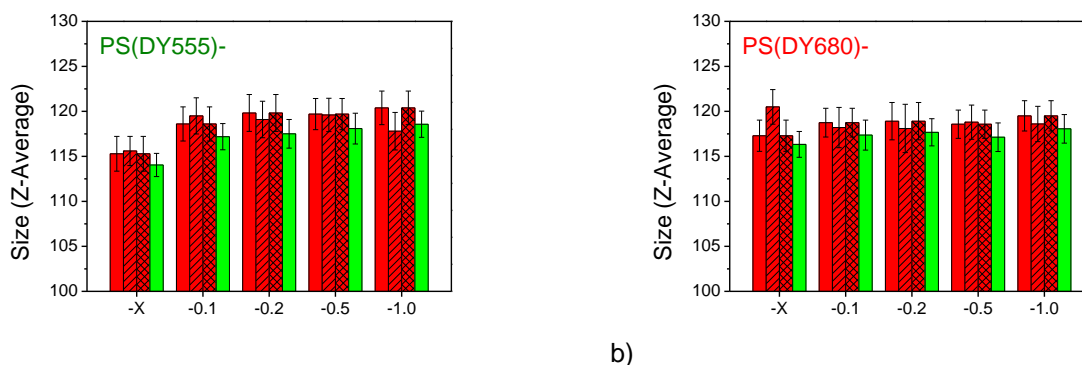


Figure 3: Size measurement results (Z-average values) of the DY555-stained (a) and DY680-stained (b) PS particles as measured with DLS using either a “red” instrument with a 633 nm laser (red bars) or a “green” instrument with a 532 nm laser (green bars). The different textures of the red bars indicate measurements carried out at three different laboratories, and the error bars denote the standard deviations of the mean of the 100 measurements after outlier removal. The measured Z-average values reveal no significant effect of the dye absorption wavelength or dye staining concentration.

Influence of biological media on zeta potential measurements

Surface charge, typically expressed in terms of the zeta potential, represents another property of nanomaterials with a big influence on their overall chemical behaviour. The most widely applied method for measurements of the zeta potential is electrophoretic light scattering (ELS), which detects the frequency shift of light which is scattered off the particles as they oscillate in an AC electric field. This technique is well established but has a drawback, as an ensemble technique, possible large variations between individual particles might disturb the measurement, especially in a biological matrix, where the interaction of the particles with the proteins leads to the formation of the protein corona and agglomerates. In addition to ELS, the two emerging techniques NTA and Tunable Resistive Pulse Sensing (TRPS) were also used by the project. In both NTA and TRPS the surface charge of particles can be determined on a particle-by-particle basis.

TRPS is an emerging technique based on the Coulter principle that measures the reduction in ionic current across a pore on a membrane due to the temporary occlusion of the pore as the particle traverses it. For zeta potential measurements, the particles move under the action of an electric field. TRPS is capable of measuring particle by particle charge by mapping the “blockade” signal when a particle passes through the nanopore and by calculating its velocity. The technique also provides a statistical distribution of the zeta potential values measured within a sample and allows the simultaneous measurement of single nanoparticle size and zeta potential.

NTA is a variant of PTA which is performed under the influence of an electric field. PTA detects scattering coming from the particles illuminated with a laser beam and tracks their movement in solution. The camera captures a video and the recorded movie is then analysed by software, which locates and tracks individual particles frame-by-frame and calculates their zeta potential from measurements of the velocity of particles in suspension when an electric field is applied (electrophoretic velocity). In contrast to PTA, NTA records the total velocity for each tracked particle, which is a sum of two motions (electrophoretic mobility and Brownian motion). By observing the total velocity at different depths within the closed sample chamber and assuming a zero net flow over the entire chamber depth, it is possible to separate these two components. The electrophoretic velocity can therefore be measured for every particle tracked by the instrument and electrophoretic velocity is then used to calculate the zeta potential on a particle-by-particle basis.

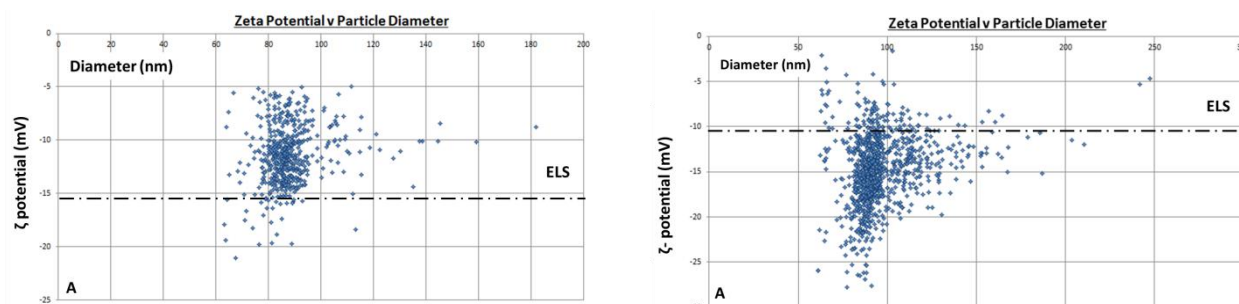


Figure 4: Measurement of the zeta potential using TRPS for RM2 in Tris-HCl buffer (left) and biological media (right). The symbols denote the zeta potential measurements for individual particles tracked by TRPS. The dashed line represents the ensemble average as obtained by ELS.

The comparison of results between TRPS, ELS and NTA was not straightforward for several reasons. One reason might be the differences in samples used in the different laboratories, at partners BAM, LGC and NPL and at different points over time. However, the homogeneity and stability data provided with the test materials i.e. RM1; amimated silica nanoparticles and RM2; plain silica nanoparticles was much smaller than the experimentally observed differences. Therefore, for the purpose of the study, the test materials can be considered as being reliable reference materials. A second reason for the variation between the measured values could be the intrinsic differences between the measurement principles of the applied methods. Both NTA and ELS are light scattering-based techniques. For the latter, the particle velocity is determined from the frequency shift using the Doppler effect, whereas for NTA both electrophoretic and Brownian motions of each particle is extracted by analysing the track of a particle in time. Drift velocities are also calculated on a particle-by-particle basis and are not intensity-weighted towards larger nanoparticles. In contrast, TRPS provides measurements which are independent of the light scattering properties of the particles and the velocity of each nanoparticle can be calculated by the analysis of their transit time through an aperture. The results obtained by TRPS indicated that particle size and ζ -potential properties can be observed and correlated. A third, reason for the experimental scatter could be due to variations in sample preparation protocols, which should be optimised for each instrument according to their technical requirements [10].

A comparison between the results obtained by TRPS and ELS is shown in **Figure 4**. The results obtained by ELS for RM2 in TRIS-HCl buffer were significantly lower than the ensemble average by TRPS. The measurement in biological medium showed the opposite trend. In TRIS-HCl buffer, the mean zeta potential value of plain silica measured by ELS was more negative than the values obtained by TRPS, while less negative for amimated silica i.e. RM1. The latter was due to the moderate dilution factor used for ELS measurements and hence a lower pH value. For measurements in bovine serum both TRPS and ELS s measured consistently negative zeta potential values for both the plain and amimated silica nanoparticles (i.e. RM2 and RM1 respectively). The ELS mean zeta potential showed less negative values for RM1, which may be due to lower pH or the presence of a small population of larger nanoparticles with a less negative zeta potential. Such particles will scatter light more intensely and will contribute disproportionately to the ELS measurement, resulting in the measured zeta potential being skewed by a subpopulation of the nanoparticles.

The results obtained by ELS and NTA in water in the case of RM1 amimated silica nanoparticles seemed to disagree, ELS measured slightly positive zeta potential values and NTA provided negative zeta potentials. However, samples for NTA measurements were considerably more dilute in purified water than those prepared for ELS measurements. A direct consequence of such dilution was the change in pH of the solution: i.e. ELS measurements were performed at pH 3.6 and NTA measurements were performed at pH 5.2. Titration studies show that, when taking the environmental pH into consideration, the ELS zeta potential results (in water at pH 5) are comparable to the NTA results.

The type of buffer and its molarity is an additional factor to be considered during zeta potential measurements. For example, TRPS measurements need to be performed in an electrolyte solution of a certain ionic strength and therefore zeta potential measurements in purified water or 50 mM Tris–HCl could not be performed, unlike

ELS and NTA. When NTA measurements were repeated in 150 mM Tris–HCl buffer, no significant difference in zeta potential was observed and therefore, a comparison amongst the measurements performed in buffer could still be attempted. Both iRM1; aminated silica nanoparticles and RM2; plain silica nanoparticles in Tris–HCl buffer exhibited a negative zeta potential as measured by all techniques. Whilst TRPS, ELS and NTA techniques were in broad agreement for the zeta potential of plain silica RM2, that of aminated silica RM1 measured by ELS was significantly less negative than that measured by both TRPS and NTA. However, it is possible that the ELS zeta potential measurements are skewed by the presence of agglomerates or agglomerates/aggregates, as when nanoparticles are introduced in serum, some of the proteins may adsorb at the surface of nanoparticles. According to Tenzer and co-workers [S. Tenzer, D. Docter, J. Kuharev, A. Musyanovych, V. Fetz, R. Hecht, F. Schlenk, D. Fischer, K. Kiouptsi, C. Reinhardt, K. Landfester, H. Schild, M. Maskos, S. K. Knauer and R. H. Stauber, *Nat. Nanotechnol.*, 2013, 8, 772–781] at physiological pH protein-coated silica nanoparticles display a negative surface charge density, irrespective of the original nanoparticles' surface charge density or duration of their exposure to human plasma proteins.

All 3 techniques, TRPS, ELS and NTA consistently measured negative zeta potential values for both the plain and aminated silica (i.e. RM2 and RM1 respectively) in FBS regardless of the difference in the concentration of the nanoparticles and bovine serum content used (due to the instrumental requirements). Zeta potential values were also similar for RM1 and RM2, although not identical, and did not significantly change with time.

Influence of particle agglomeration state on the number-based concentration measurements in biological media

Determination of number-based particle concentration is one of the requirements of recent European Union legislation. However, there are many challenges associated with the number-based measurements of particles in a complex product or biological matrices. One of them is a potential aggregation/agglomeration of nanomaterials upon interaction with matrix components, as often seen in biological media. Under such circumstances, the individual nanoparticles forming an aggregate or agglomerate are no longer counted, but the entire structure is taken as one object, and consequently substantially lower particle concentrations are determined, unlike for mass-based analysis. Therefore, in order to fully understand and interpret number-based particle concentration data, it is important to also determine the materials' aggregation/agglomeration state.

The influence of particle agglomeration/aggregation on concentration measurements was studied in serum-containing biological media with PTA, TRPS and asymmetric flow field flow fractionation (AF4) online coupled to multi-angle light scattering (MALS) and inductively coupled plasma mass spectrometry (ICP-MS) (i.e. AF4/MALS/ICP-MS). These 3 techniques were selected because they are not only capable of particle size and size distribution determination in solution, but also of number-based particle concentration determination, either directly (PTA and TRPS) or through signal conversion from mass fraction to particle number (AF4/MALS/ICP-MS). RM1 (aminated colloidal silica) and RM2 (plain colloidal silica) nanomaterials were dispersed in cell culture medium containing 10% foetal bovine serum (FBS), following the protocol developed by LGC and at a dilution appropriate for the technique. Measurements were performed immediately after the suspensions were prepared and following 24 hour incubation at room temperature.

The results of the measurements are shown in **Figure 5**. The agglomerates are indicated by arrows in these graphs. Results showed that RM2 was stable over 24h incubation time in biological media i.e. the agglomeration state as detected by these methods did not change. RM1 was found to agglomerate/aggregate overtime, with substantial proportion of dimers compared to monomers. Since, the exact diameter of agglomerates/aggregates measured is technique specific, care should be taken when interpreting the comparative agglomeration state data.

The effect of particle agglomeration/aggregation on concentration measurements was then assessed. Both, PTA and TRPS measure particle concentration in number-based terms directly, whilst the AF4/ICP-MS provides the mass fraction of silicon, which could be converted to equivalent particle number. The signal from the MALS detector, despite being useful for sample agglomeration assessment, was found unsuitable for reliable concentration determination, with a standard deviation between measurements of up to 30 %.

These results on concentration measurements are summarised in **Figure 6**. The particle concentration counts varied depending on the technique, due to losses of material during measurements, with the highest recovery rates (value the closest to expected) observed for PTA. Despite these differences, the observed trend was a good agreement between the techniques, with significantly lower counts seen for the aminated material (i.e. RM1) after 24h incubation than in any other sample, which was correlated with the formation of agglomerates/aggregates.

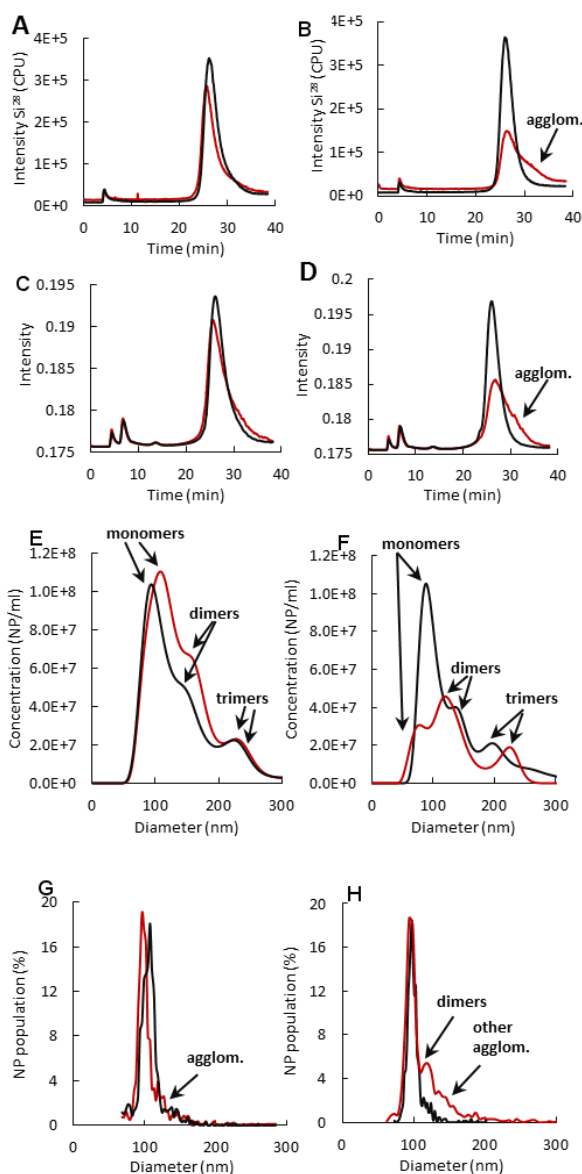


Figure 5: Comparison of the agglomeration state between AF4/ICP-MS (A and B), AF4/MALS (C and D), NTA (E and F), and TRPS (G and H). Measurements were taken immediately after dispersion (left) and after 24 h incubation at room temperature (right) of RM1 (plain silica, black) and RM2 (aminated silica, red) in cell culture medium. Arrows indicate agglomerates.

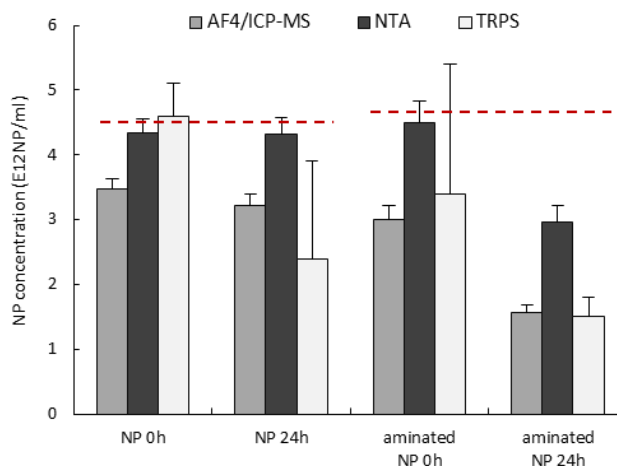


Figure 6: Number-based concentration measurements of SiO₂ NP suspended in biological media, as detected by various methods. Red dashed lines represent the expected values from a mass balance equation taking into account the total Si content and the core size of the NPs from TEM.

Conclusions

Multiple physical and chemical methodologies were developed and validated. Then, through a series of inter-laboratory studies, the size, size distribution, surface charge, concentration (chemical composition) and agglomeration of the plain colloidal silica and NH₃-modified colloidal silica reference nanomaterials were characterised in water, buffered aqueous solutions (e.g. Tris-HCl buffer solutions) and biological serum. The methods used included small-angle X-ray scattering (SAXS), field flow fractionation coupled with multi-angle light scattering (FFF/MALS), differential scanning calorimetry (DCS), dynamic light scattering (DLS) and nanoparticle tracking analysis (NTA).

The objective was successfully achieved, as the effect of the biological medium and fluorescent staining on size measurements, and the influence of particle agglomeration (caused by the biological media) on number-based concentration measurements has been evaluated for the first time. In addition, the first method for determining the concentration of silica nanoparticles in a biological matrix using NTA has been developed. The potential benefits and drawbacks of the different techniques used (SAXS, FFF/MALS, DCS, DLS and NTA) were also summarised and published (see Sikora *et al.* 2015 in the list of publications section 6).

3.3 Objective 3: Development of methods for the simultaneous characterisation of physical and chemical composition of nanomaterials in cell based biological systems.

The aim of this work was to use the reference materials from objective 1 to develop real-time measurement of physical and chemical properties in a cell-based biological system. In particular, to develop methods for the simultaneous characterisation of physical and chemical composition of nanomaterials in cell based biological systems.

Determination of total and 'nano' mass fraction of silicon

RM1 and RM2 aqueous and biological media suspensions were analysed for the total content of silicon (Si) mass fraction by isotope dilution mass spectrometry (IDMS), which is recognised as a primary ratio method for the determination of the amount of substance. A bracketing, exact matching double IDMS method was used (**Equation 3.1**), which minimises the effects of instrument detector linearity and spike calibration, and with this approach, both the sample and a primary elemental standard are spiked with an enriched isotope (^{29}Si) to give isotope ratio of $^{28}\text{Si}/^{29}\text{Si}$ close to 1.

$$C'_x = \lambda \cdot C_z \cdot \frac{m_Y}{m_X} \cdot \frac{m_{Zc}}{m_{Yc}} \cdot \frac{R_Y - R'_B \cdot \frac{R_{Bc}}{R'_{Bc}}}{R'_B \cdot \frac{R_{Bc}}{R'_{Bc}} - R_X} \cdot \frac{R_{Bc} - R_Z}{R_Y - R_{Bc}} \cdot \frac{\sum R_{ix}}{\sum R_{iz}} \quad \text{Equation 3.1}$$

Where, C'_x is a mass fraction of analyte in sample X obtained from one measurement; C_z – mass fraction of analyte in primary standard Z; m_Y – mass of spike Y added to sample X to prepare the blend B (=X+Y); m_X – mass of sample X added to the spike Y to prepare the blend B (=X+Y); m_{Zc} – mass of primary standard solution Z added to the spike Y to make the calibration blend Bc (Bc=Y+Z); m_{Yc} – mass of spike Y added to the primary standard solution Z to make the calibration blend Bc; R'_B – measured isotope amount ratio of the sample blend B; R'_{Bc} – measured isotope amount ratio of the calibration blend Bc; R_{Bc} – gravimetric value of the isotope amount ratio of the calibration blend; R_X – isotope amount ratio of sample X; R_Z – isotope amount ratio of primary standard Z (certified value); $\sum R_{ix}$ – sum of isotope amount ratios in sample X; $\sum R_{iz}$ – sum of isotope amount ratios in primary standard Z (certified value). Blend to blend variation (λ) was included in uncertainty calculation only (i.e. the value = 1 but with an associated uncertainty).

To determine the mass of silicon in the 'nano' fraction, samples eluted from the field flow fractionation (FFF) channel were quantified for their element content by a post-channel calibration approach. In this post-channel calibration approach, the post-column diluting nitric acid/internal standard mix was replaced with calibration standards, containing the same amount of nitric acid and an internal standard (germanium (Ge), m/z 72 was monitored) but increasing concentrations of elemental silicon (m/z 28 and m/z 29 were monitored). Elemental rather than a particulate form of silicon was used as the calibrant, as this is the only type of reference material certified for silicon content available on the market at the time the experiments were performed. The same flow rates going into the nebuliser were used during the calibration step and sample analysis. AF4 fractograms normalised against internal standard were converted into mass flow fractograms using a calculation from the calibration curve regression parameters and measured sample flow rates. The total peak area present in the background corrected fractograms was calculated using a sum of trapezoid approximation and the concentration of silicon in the sample was calculated from the total injected volume and dilution factor of the injected sample.

As an alternative to the post-channel calibration approach, silicon content in the 'nano' fraction eluting from the FFF channel of the RM2 material, as well a sample of natural Ströber silica particles synthesised in-house was determined using particle-specific, bracketing, exact matching double IDMS, following **Equation 3.1**, which minimises the effects of instrument detector linearity and spike calibration. In this IDMS methodology, isotopically (^{29}Si) enriched Ströber silica particles, with an average size of about 80nm were used as a spike. The spike was mixed with the sample (either RM2 or natural Ströber silica particles) to form a sample blend containing a ratio of $^{28}\text{Si}/^{29}\text{Si}$ isotopes close to 1.5, which was found to be optimal for the developed method.

Alongside the sample blend, a calibration blend, containing the spike and a calibrant (RM2) was prepared in an analogous way (with a difference in ratio between blends of less than 5 %).

The amount of silicon in the RM2 material quantified using the particle-specific IDMS developed in the project, agreed within the level of uncertainty of the amount of silicon in the RM2 material measured using total IDMS, as shown in Figure 11. These results suggest that the only source of silicon in this material is the nano fraction. In contrast, the amount of silicon in an RM2 water suspension quantified using the post-channel quantification approach was significantly lower ($853.3 \pm 64.6 \mu\text{g/g}$, average \pm stdev, $n=9$). This difference was related to the losses of the material in the AF4 system during separation (around 13 %, most likely due to particle 'sticking' to the FFF membrane) and to a different ionisation efficiency of the nanoparticulate (analyte) and elemental (calibrant) form of silicon (around 10-15 % difference, depending on the matrix). These issues were not present in particle-specific IDMS, as elemental silicon is not used, in addition losses of the sample and the calibrant in the AF4 system are the same and were therefore cancelled out. In case of the natural Ströber silica sample the quantified amount of silicon by total and particle-specific IDMS were significantly different. This indicates that there are other than 'nano' sources of silicon in the sample (e.g. unreacted sources leftover after the synthesis precursor) and shows that total element quantification can lead to overestimation of the amount of silicon in the nanoparticulate form. No influence of biological media (10% FBS at 10-fold dilution) on the total IDMS method was found for RM2 and RM1 materials, as opposed to the post-channel calibration approach, where the biological matrix was found to minimise losses of the RM1 material in the FFF system during separation (with no significant effect on RM2 seen).

Analyte	Method	Mean ($\mu\text{g/g}$)	U, k=2 ($\mu\text{g/g}$)	RSU (%)
RM2	Total IDMS	1108	14.4	1.3
	Particle-specific IDMS	1094	9.15	0.8
Ströber silica	Total IDMS	5597	108	1.9
	Particle-specific IDMS	5143	199	3.9

Figure 7: Total ($n=12-25$) and size-resolved ($n=9$) IDMS results.

Determination of number-based particle content

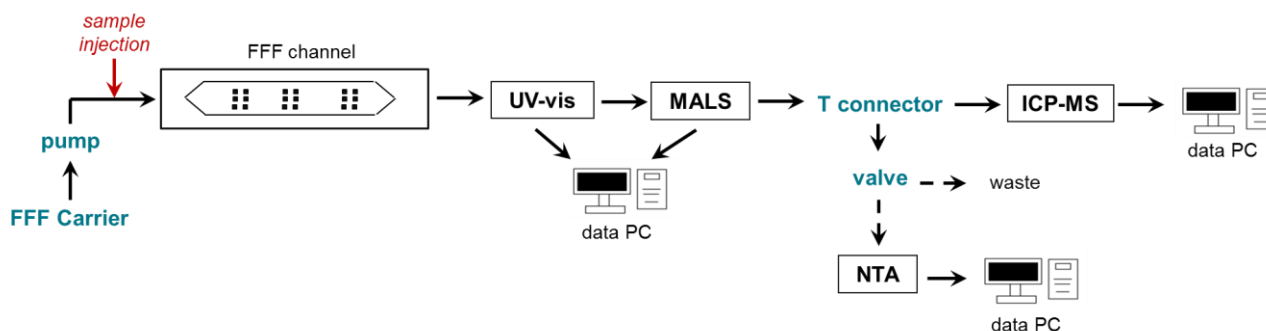


Figure 8: Schematic diagram representing on-line NTA coupling to FFF/MALS/ICP-MS.

For the first time ever this project investigated, the potential of simultaneous on-line coupling of FFF to NTA, ICP-MS and MALS for the physicochemical characterisation of silica particles suspended in a bovine serum matrix. The on-line system was assembled as shown in **Figure 8**. An additional T connector and a software-controlled switching valve were also introduced into a typical FFF/MALS/ICP-MS system, allowing coupling of the NTA platform and a stop-flow operation (dashed line) in an on-line mode. The degree of selectivity offered by FFF was found in order to determine the number-based concentration of particles (using RM1 as an example) suspended in biological serum with a relative standard deviation of 5.1 % ($n=3$). ICP-MS analysis of FFF size fractions provided information on particle mass concentration for example, from the Si mass fraction obtained with the post-channel calibration approach, the equivalent number of particles was estimated,

assuming around 80nm particle core diameter and around 2g/cm³ density. The results also showed that measurements with NTA (4.1 ± 0.21) 10¹² NP/g number of particles agreed well with the estimated number from FFF/ICP-MS measurements (4.4 ± 0.21) 10¹² NP/g, provided that losses in the FFF system as well as differences in the nebulisation efficiency between the particulate and elemental form of silicon were accounted for.

Particle size analysis with MALS detector

The average size of particles was estimated using direct and indirect approaches with a MALS detector (**Figure 9**). In the direct approach the size of particles in a fraction is calculated with the FFF software from the intensity of the scattered light at 18 out of 21 available angles using a sphere fit model. The indirect approach is based on the sample elution time from the system and the particle size is calculated from a calibration curve obtained with the same FFF method for a known particle standard (ERM-FD102 from partner JRC; however, please note that this reference material is not certified for such use). Size values obtained at 0 h time point using both the direct and indirect approaches with a MALS detector agree well with each other and with the other methods used in objective 2. In Tris-HCl buffer RM1 and RM2 showed size just under 80nm, whilst in biological media their diameter increased to about 90nm, caused by the protein corona formation. In the case of FFF/MALS only the so called 'hard corona' was seen, since the excess of unbound as well as weakly interacting proteins was removed from the sample during separation. In contrast, NTA also measures the 'soft corona', which is the reason why the diameter of particles is larger (around 100nm). As opposed to MALS and NTA, SAXS and DCS cannot see the protein corona at all (obtained size values were about 80nm). In a water environment, the size of RM2 was very similar to the value obtained in Tris-HCl buffer, but the diameter of RM1 is slightly larger (around 85 nm). This could be explained by formation of small agglomerates/aggregates in the water environment, evident from the tailing of the main fraction peak (see objective 2 for more details on agglomerates/aggregates). Amination (i.e. RM1) brought the particles surface charge close to neutral (from strong negative charge seen for plain silica (i.e. RM2));, which is known to destabilise colloids, especially when the particles are forced close together, as per during the focusing step. In buffered environment and in biological media RM1 showed stronger charge, which alongside the formation of protein corona offering a steric hindrance, increases the particles stability against agglomeration/aggregation.

As opposed to the direct approach, no significant differences were found for size values of RM1 in water after 0 h and 24 h incubation obtained with the indirect approach. This is because the elution time of the main size fraction (monomers) was not changed. The reason why different size values were obtained using the direct approach is that the whole peak, including tailing representative of aggregates/agglomerates (more pronounced after 24 h) was taken under consideration when calculating the average particle size.

Method	Material	Time point	Diameter (nm)		
			water	Tris	Media
Direct	RM1	0h	86.2 ± 4.7	77.7 ± 1.7	90.3 ± 3.6
	RM2		76.6 ± 5.8	75.4 ± 2.2	90.7 ± 3.4
Indirect	RM1		84.2 ± 5.3	78.7 ± 1.9	87.1 ± 0.9
	RM2		74.6 ± 3.1	77.1 ± 4.9	87.2 ± 1.1
Direct	RM1	24h	95.8 ± 4.2	75.4 ± 1.4	93.4 ± 4.7
	RM2		74.8 ± 1.8	79.5 ± 1.7	92.4 ± 3.6
Indirect	RM1		85.2 ± 1.8	77.1 ± 6.1	88.8 ± 1.8
	RM2		77.8 ± 3.96	73.8 ± 1.9	87.8 ± 0.6

Figure 9: Size values obtained for RM1 and RM2 using direct and indirect sizing approaches with MALS detector (average \pm stdev, n=9).

Combined X-ray techniques for simultaneous determination of size, size distribution and chemical composition of nanomaterials in biological systems

The aim of combined SAXS and X-ray fluorescence (XRF) measurements on nanomaterials in biological media was to simultaneously obtain information on the size as well as about the chemical composition of the studied samples. For sufficiently monodisperse nanomaterials, SAXS can be used for traceable size determination. Whereas XRF is based on the emission of fluorescent X-ray photons upon excitation of the electrons in the studied sample with X-ray radiation. Since the energies of the emitted photons are characteristic to the constituent atoms of the sample, XRF can provide information on the chemical composition. ASAXS combines the elastic scattering of X-ray photons on the electrons with the inelastic processes occurring at X-ray energies near to the absorption edge of the element under consideration. In this way ASAXS can provide element specific structural information on a multicomponent system.

When nanomaterials are mixed with a complex biological matrix, the multicomponent nature of those samples could disturb the size measurements due to scattering from the nanomaterials and the matrix. However, for many engineered nanomaterials with a relatively high density, including the the nanoparticles chosen for this project, SAXS alone is capable of determining the size distribution of the nanomaterials even in 60% biological serum. This can be explained by the fact that the electron density contrast of the nanomaterials, and hence the scattering signal, is much higher than that of the components of the biological matrix. However, in order to demonstrate the capabilities of ASAXS in the determination of the size of nanomaterials in a complex matrix, mixtures of RM2 and Titanium (TiO_2), which creates a strong background, were studied. A summary of the ASAXS results on this mixture is given below, followed by the results on the XRF measurements on the silica nanomaterials mixed with cell lysate and simultaneous SAXS measurements.

In order to be able to perform ASAXS and XRF experiments at light elements of technical and biological relevance, it was necessary to go to photon energies below 5 keV. Several technical difficulties had to be overcome to achieve this. At these energies, experiments must be carried out in a vacuum because of the scattering and attenuation of the radiation in air. The radiation is also absorbed in the sample within a few hundred micrometres, therefore a liquid sample holder is necessary which encloses a thin sheet of the sample liquid between X-ray transparent windows and is vacuum proof. The sample holder which was developed by the project for a photon energy range from 3 keV to 6 keV is depicted in **Figure 10a**. For the detection of the scattered radiation a PILATUS scattering detector was modified to operate directly in vacuum, which is shown in **Figure 10b**. This setup is now in routine operation at the FCM beamline of project partner PTB at the synchrotron radiation facility BESSY II in Berlin.

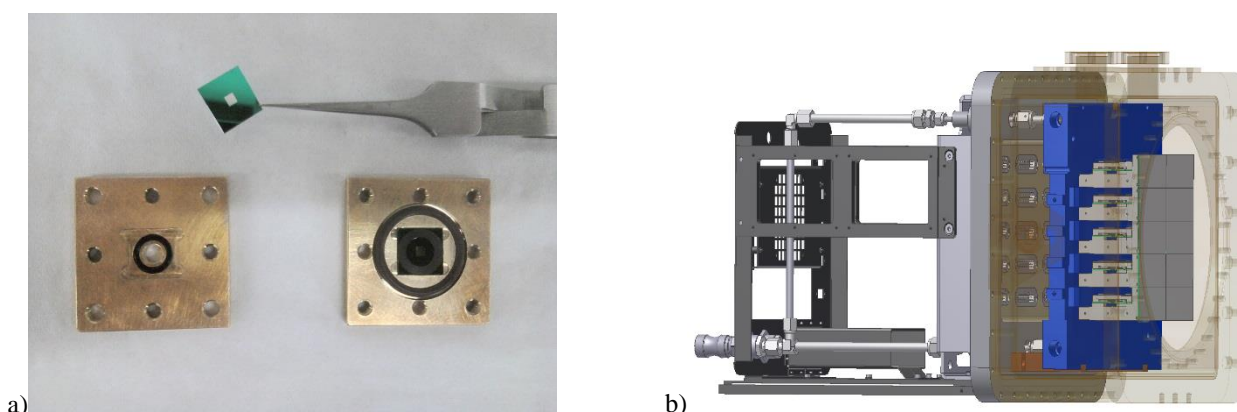


Figure 10: The liquid sample holder (a) and the vacuum proof scattering detector (b) used for simultaneous XRF and ASAXS measurements at the FCM beamline of PTB.

Figure 11 (left) shows the result of a single SAXS measurement of RM2 mixed with TiO_2 particles. Due to the high electron density contrast and broad size distribution of the TiO_2 particles, they induced a strong background scattering which hindered the accurate size determination from the simple SAXS measurement. However, measuring the scattering curves at different energies below the absorption edge of titanium (ASAXS curves) enabled the separation of the scattering contribution of the silica particles **Figure 11 (right)**. The measured ASAXS curves differed in the contribution of the TiO_2 to the total scattering, therefore the scattering

of the silica particles could be separated by a subtraction taking into account the changes in the effective electron density contrasts of the different constituents of the sample.

From the fit to the separated scattering of the silica particles (ASAXS) a diameter of 80.48 ± 2.05 (1σ) nm was obtained, while from the fit to the full SAXS curve of the nanoparticle mixture results of 64.42 ± 19.92 (1σ) nm were obtained. Although both values agreed with the size determined from the pure RM2 within the stated standard uncertainties (81.1 ± 0.7) nm, this clearly indicates that in the case of the silica-TiO₂ mixture SAXS was not capable of accurate size determination, whereas the ASAXS analysis was able to reveal the size of the silica particles with small uncertainties.

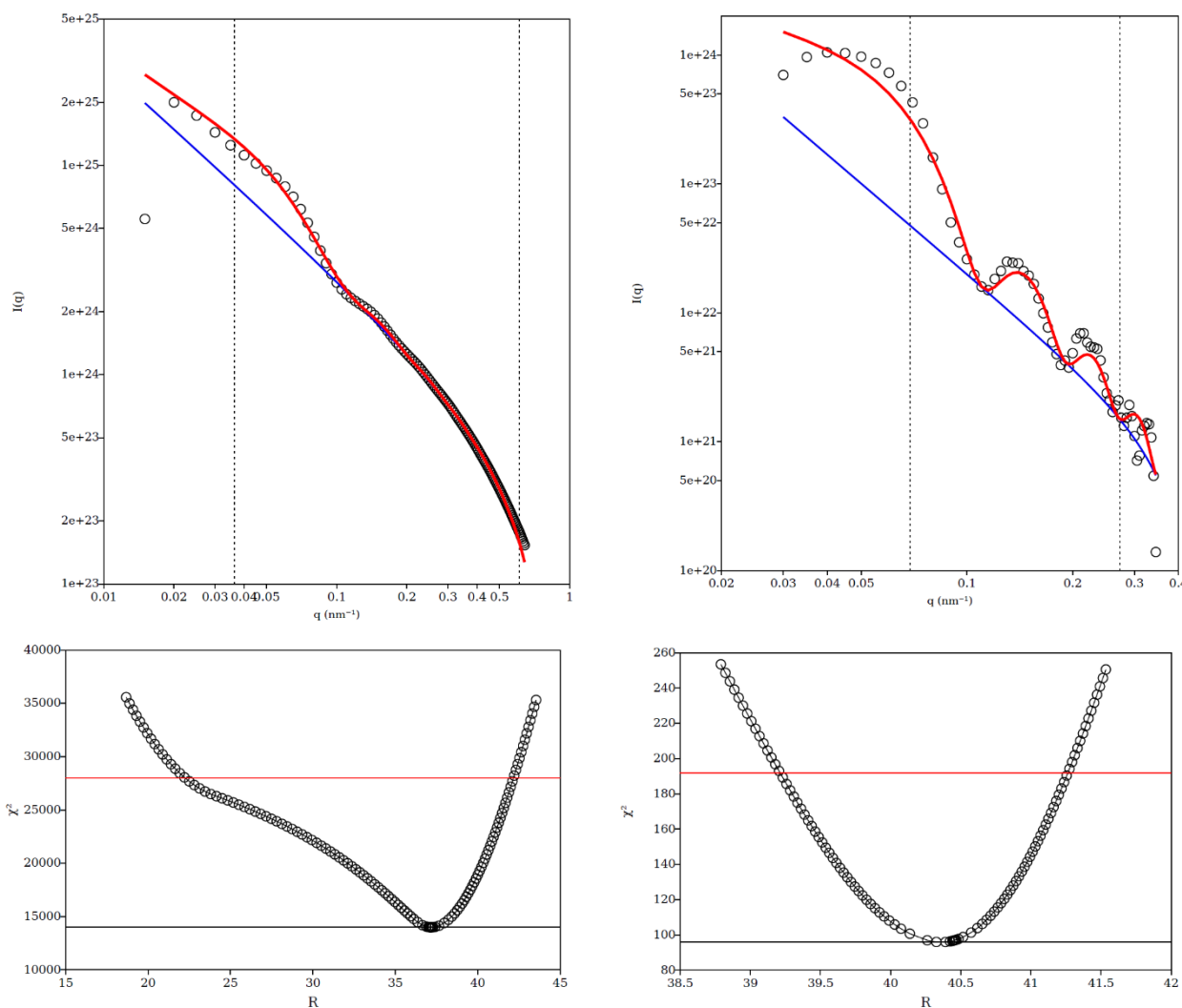


Figure 11: SAXS curve of the RM2-TiO₂ sample together with the best model fit (left) and the separated scattering curve of the silica particles from ASAXS analysis together with the best model fit (right). Uncertainty scans for the obtained radius are shown below the scattering curves.

The results of combined SAXS and XRF measurements on RM1 mixed with cell lysates is shown in **Figure 12**. As in the case of the cell culture medium, the size of the particles can be obtained from the SAXS measurements (**Figure 12a**) by model fitting (red line) without special treatment. The resulting diameters agreed with those for the particles dispersed in water within their stated standard uncertainties. Additional information about the agglomeration state of the particles was obtained from the low- q part of the scattering curves. Here, the fitted theoretical scattering curves deviated from the measured data points in the low q -range, which indicated agglomeration of the particles. The XRF spectrum of the same sample is shown in

Figure 12b. Characteristic peaks corresponding to the biological matrix (sulphur), the used buffer (chlorine), and the nanomaterials (Si), can be clearly identified. However the latter peak cannot be used for the accurate quantification of the silica content because of the use of SiN windows. In contrast XRF can be used for the quantification of the protein content of the sample based on the fluorescence peak of sulphur, as absolute protein concentration of an unknown sample can be obtained by measuring reference samples with known protein concentrations.

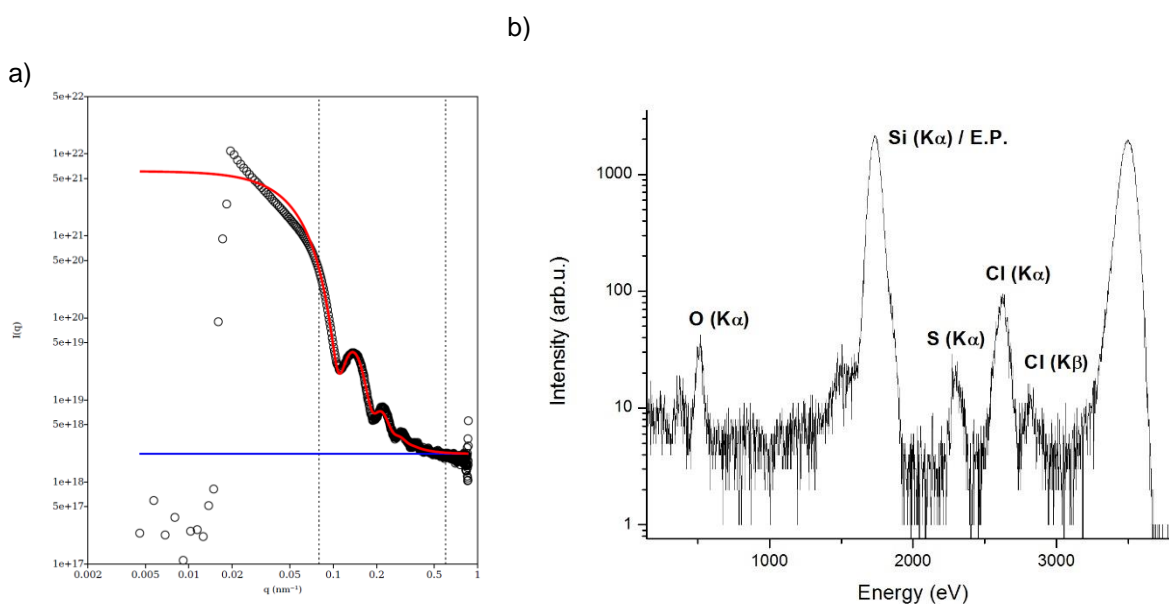


Figure 12: SAXS (a) and XRF(b) measurements on RM1 mixed with cell lysate for simultaneous physical and chemical characterisation, respectively.

Conclusions

To address the need for real-time physical and chemical characterisation of nanomaterials in biological samples, a novel methodology combining FFF with inductively coupled plasma mass spectrometry (ICP-MS) was developed and validated to measure chemical composition and size. The project produced, for the first time, silica nanoparticles isotopically enriched with ^{29}Si , and used them for accurate size-specific isotope dilution quantification (SI traceable) in aqueous suspensions using FFF-ICP-MS, with an expanded uncertainty of approximately 3.9%. The objective was achieved, and this measurement capability is invaluable for future chemical characterisation of reference nanomaterials. The know-how gathered on the method development and validation was also included in the BSI Publicly Available Specification (PAS) 139 guidelines (Detection and characterisation of nanomaterials in biological samples).

3.4 Objective 4: Development of traceable methods for the characterisation of ‘bulk’ optical properties of fluorescent nanomaterials, in particular quantum yield, absorption coefficient and corrected emission spectra.

The aim of this work was to use the reference materials from objective 1 to measure the optical properties of fluorescent nanomaterials in a serum-based system. More specifically, to develop traceable methods for the characterisation of ‘bulk’ optical properties of fluorescent nanomaterials, in particular quantum yield, absorption coefficient and corrected emission spectra.

Quantum yields (QY) of spectral fluorescent standards and QY standards

As a first step towards traceable, relative and absolute quantum yield (QY) measurements, two different integrating sphere setups at project partners BAM and PTB were extensively characterised and compared. BAM used a custom-built stand-alone integrating sphere setup consisting of a 150 mm-sized integrating sphere fibre-coupled to a Charge Coupled Device (CCD)-based detector, whereas PTB used a custom-made 80 mm-sized integrating sphere accessory-integrated into the sample chamber of a common Horiba JobinYvon spectrometer. Spectral fluorescence standards and QY standards to be used for the integrating sphere comparison were identified, including the commercially available BAM-certified spectral fluorescence standard kit dyes F002-F005, and commonly used QY standards, such as rhodamine 6G (Rh6G), rhodamine 101 (Rh101), and oxazine 1 (Oxa1). The absorption and emission spectra of the chosen fluorescent standard dyes are shown in **Figure 13**.

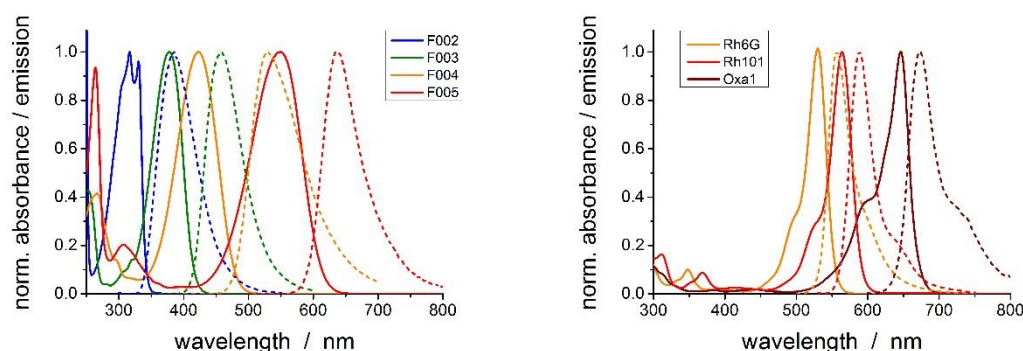


Figure 13: Normalised absorbance spectra and intensity-corrected emission spectra of the BAM-certified spectral fluorescence standard kit dyes F002-F005 (left) and common QY standards (right).

By applying the selected dye standards and agreed protocols for traceable, relative and absolute QY measurements of transparent (non-scattering) dye solutions, the two different integrating sphere setups at BAM and PTB were characterised and compared regarding their relative spectral responsivity, dynamic sensitivity range, and degree of reabsorption (inner filter) effects. The relative spectral responsivities of both integrating sphere set-ups covered the wavelength range from 400-750 nm with deviations below 4 % using the BAM-certified emission spectra (only the PTB- integrating sphere set-up showed slightly larger deviations of up to 10% at wavelengths of 550-625 nm). Regarding the dynamic sensitivity ranges, the BAM- integrating sphere set-up could reproducibly measure the QY values of Rh101 in the concentration range from ca. $1 \cdot 10^{-5}$ M (OD = 1.0) to ca. $2.5 \cdot 10^{-7}$ M (OD = 0.025), whereas the PTB- integrating sphere set-up could not measure concentrations below $1 \cdot 10^{-6}$ M (below OD = 0.1), most likely due to a lower sensitivity of the detector (i.e. lower signal-to-noise ratios). For both integrating sphere set-ups, a reabsorption correction was necessary at higher Rh101 dye concentrations, to account for inner filter effects.

The QY values of the spectral fluorescence standards and working QY standards were then measured with both integrating sphere setups. The results, summarised in **Figure 14**, were in good agreement between the different integrating sphere setups and with the respective literature values.

Dye	BAM	PTB
F002	---	0.25
F003	0.48	0.49
F004	0.53	0.55
F005	0.64	0.66
Rh6G	0.91	0.94
Rh101	0.92	0.94
Oxa1	0.15	0.13

Figure 14: QY values of the BAM-certified spectral fluorescence standard kit dyes F002-F005 and the common QY standards rhodamine 6G (Rh6G), rhodamine 101 (Rh101) and oxazine 1 (Oxa1) as measured absolutely with the different integrating sphere setups and BAM and PTB.

Lastly, the sources contributing to the uncertainties of relative and absolute QY measurements were assessed, and the corresponding uncertainty budgets were provided. Two relative methods (same excitation wavelength for standard and sample vs. different excitation wavelengths for standard and sample including excitation correction) and one absolute method (integrating sphere measurement) for the optical QY determination of fluorescent standards were examined. With all three methods, uncertainties below 7 % could be achieved if typical calibration- and measurement-inherent uncertainty sources were minimised. For the most commonly used relative methods, the reliability of the QY value of the standard was identified by the project as the key source of systematic variation, and for relative QY measurements, using the same excitation wavelength for standards and samples is recommended by the project as the method of choice. Using different excitation wavelengths for the standard and sample might be more flexible, however low uncertainties can only be accomplished if excitation calibration-related uncertainties are minimised. Further to this, the use of emission and excitation correction curves implemented by instrument manufacturers is only recommended if all parameters (determination method, instrument settings, radiometric reference quantities) are known, and it should be evaluated prior to their application. Finally, for absolute QY measurements using the integrating sphere setup at BAM, relative measurement and calibration related uncertainties of around 3 % were determined.

Quantum yields of fluorescent nanomaterials in different media

The characterised integrating sphere setups at BAM and PTB were used to determine the QY values of nanomaterials FM1-FM4 and RM3 in aqueous media and biological serum, using the common dispersion protocol developed at LGC. Relative QY measurements were not applicable, due to significant scattering of the particle samples and the biological serum. The absorption and emission spectra of the fluorescent nanomaterials i.e FM1-FM4 in ultrapure water are displayed in **Figure 15**. For comparison, the fluorescent dyes DY557 (used to produce FM1/2) and DY680 (used to produce FM3/4) were also measured.

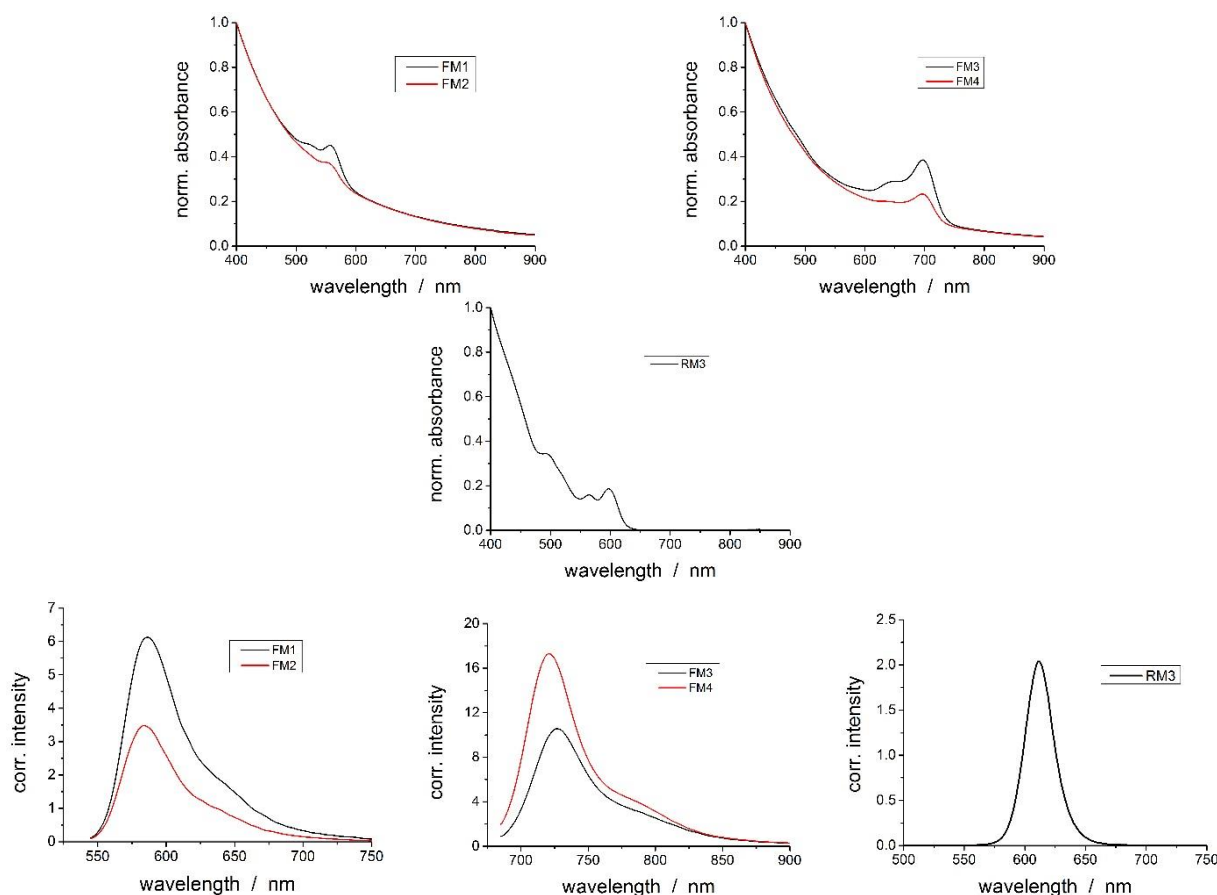


Figure 15: Normalised absorbance spectra (normalised to unity at 400 nm) and intensity-corrected emission spectra of the fluorescent nanomaterials FM1/2 (dye-labelled silica nanomaterials) and FM3/4 (dye-stained polymer particles) in ultrapure water.

The obtained absolute QY values are summarised in **Figure 16**. Whereas, DY680, FM3 and RM3 showed a significant dependence of their QY on the dispersant media (i.e. a strong increase in QY in serum compared to water and buffer), DY557 and FM4 maintained their high QY independently of the solvent even in biological serum; which makes DY557 and FM4 suitable for cellular imaging and biological assays. The results of BAM and PTB and their different integrating sphere setups were in good agreement for the transparent dye and RM3 samples and the low scattering FM1 and FM2 particles in aqueous media. However, significant deviations between the BAM-integrating sphere set-up and the PTB-integrating sphere set-up were obtained for the highly scattering particle samples in biological serum.

Dye	Solvent	BAM	PTB
DY557	Water	0.58	0.58
	Buffer	0.60	0.57
	Serum	0.53	0.60
FM1	Water	0.35	0.35
FM2	Water	0.44	0.36
DY680	Water	0.12	0.09
	Buffer	0.12	0.12
	Serum	0.35	(0.17)
FM3	Water	0.16	0.09

	Buffer	0.19	0.13
	Serum	0.37	(0.13)
FM4	Water	0.43	0.34
	Buffer	0.43	0.39
	Serum	0.43	0.39
RM3	Water	0.14	0.14
	Buffer	0.14	0.12
	Serum	0.32	(0.20)

Figure 16: QY values of the fluorescent nanomaterials FM1/2 (dye-labelled silica nanomaterials) and FM3/4 (dye-stained polymer particles), the respective dyes used to produce the fluorescent particles, and the quantum dots RM3 in ultrapure water, 50 mM Tris buffer (pH 7.4) and fetal bovine serum (FBS), as measured absolutely with the different integrating sphere setups and BAM and PTB.

The assessment of uncertainty sources for absolute QY measurements with the BAM and PTB integrating sphere setups revealed that deviations were due to the different susceptibility of the different integrating sphere setups to the influence of light redistribution caused by sample scattering upon direct sample illumination. With the sample scattering upon direct sample illumination this leads to an overestimation of the number of absorbed photons and thus an underestimation of QY. However, for indirect sample illumination the influence of scattering on the number of absorbed photons and the QY values is significantly reduced. This is due to a uniform photon distribution within the integrating sphere. Therefore the project recommends that, indirect sample illumination is used for accurate QY measurements of highly scattering samples.

Selected analytical parameters of fluorescent nanomaterials

The project developed different spectroscopic methods for the determination of other analytical parameters affecting the signalling behaviour of the fluorescent nanomaterials FM1 and/or FM2 and FM3 and/or FM4, such as the number of fluorophores, surface functional groups, or proteins (antibodies) per nanoparticle..

The numbers of fluorophores per particle were determined by absorption spectroscopy with the following 4 different methods:

1. Scatter-corrected absorption spectra of the dye-stained/-labelled particles
2. Difference of the dye amounts applied for particle labelling/staining and the amounts of unreacted/free dye within the supernatants obtained during particle preparation
3. Dissolution of the polymeric particles with Dimethylformamide (DMF) (only for FM3/4)
4. Washing of the polymeric particles with ethyl alcohol (EtOH) (only for FM3/4)

All 4 methods could be successfully applied, yielding a dye content of 130 ± 40 DY556 and 100 ± 20 DY557 labelled covalently to the aminated silica particles FM1 and FM2, respectively, as well as 7000 ± 1100 and 3800 ± 1900 DY680 sterically incorporated within the polystyrene particles FM3 and FM4, respectively.

The numbers of surface functional groups (-COOH or -NH₂) per particle were also measured with various analytical techniques:

1. Conductometric titration (for all aminated and carboxylated particles)
2. Ni²⁺/Pyrocatechol violet (PV) assay (for carboxylated particles only; addition of Ni²⁺, separation of Ni²⁺ adsorbed to the nanoparticles surface and free Ni²⁺ in the supernatant, addition of the metal ion indicator PV and its detection via absorption measurement)
3. SPDP assay (for aminated particles only; reaction with succinimidyl 3-(2-pyridylthio)propionate (SPDP), subsequent reductive cleavage with tris(2-carboxyethyl)phosphine (TCEP), and detection of the cleaved pyridine-2-thione (P2T) via absorption measurement)

4. Ellman's test (for thiolated particles or aminated particles after SPDP assay (validation of SPDP assay); reaction with 3,3'-dithio-bis(6-nitrobenzoic acid) (DTNB), and detection of the resulting 2-nitro-5-thiobenzoate anion (TNB²⁻) via absorption measurement)

With conductometric titration (415 ± 40) nmol/mg and (1060 ± 110) nmol/mg functional groups were detected on the PS-COOH and PS-NH₂ particles (used to prepare the fluorescent particles FM3 and FM4), respectively, and (470 ± 80) nmol/mg NH₂ groups were found on the aminated silica particles RM1. Applying the Ni²⁺/PV assay, (70 ± 70) nmol/mg COOH groups were detected on the carboxylated PS particles. With the combination of SPDP assay and Ellman's test, (80 ± 2) nmol/mg NH₂ groups were found on the aminated PS particles, and (5 ± 1) nmol/mg NH₂ groups were found on the aminated silica particles RM1. The reason for the higher values obtained with conductometric titration is that conductometry detects all protonable/deprotonable groups, whereas adsorption/desorption-based assays and labelling-based assays detect only the functional groups accessible for (bio-) conjugation. Thus, the latter ones were recommended by the project for estimating the number of fluorophores or biomolecules that can be attached to nanoparticles.

The numbers of anti-IL6 antibodies per fluorescent nanomaterial following bio-conjugation were determined using bicinchoninic acid (BCA) assays. The dye-stained polymeric particles FM3/4 were compared to commercially available, yellow-green (YG) and dark-red (DR) emitting fluorescent beads of 100 nm or 200 nm in diameter. Anti-IL6 antibodies were used, as Interleukin 6 (IL6) is an important biomarker for the diagnosis of many inflammatory diseases. The BCA assays revealed that all particles could be successfully bio-functionalised with anti-IL6 antibodies (ABs) using either ethyl(dimethylaminopropyl) carbodiimide (EDC)/N-Hydroxysuccinimide (NHS) chemistry for the carboxylated particles (YG100, YG200, DR200, and FM3), or NHS-Polyethylene glycol (PEG)-Maleimide cross-linkers for the aminated particles (FM4). The commercially YG100 and YG200 particles were labelled with 107 ± 1 and 1740 ± 11 ABs per particle, respectively, whereas FM3 and FM4 were functionalised with 33 ± 4 ABs and 24 ± 3 ABs per particle, respectively.

Later in the project, the measured optical and analytical particle properties were correlated with the outcome of lateral flow bioassays using the fluorescent particles FM1-4 as reporters for the quantitative detection of IL6, in order to assess the sources of uncertainty for particle-based bioassays. The following possible sources of uncertainties of lateral flow assays with fluorescent nanoparticle reporters were identified:

1. Nanoparticle-antibody conjugate-specific uncertainties:
 - Amount of dye loaded
 - Photoluminescence quantum yield
 - Functional chemistry groups on surface (reactive?)
 - Amount of antibody bound
 - Activity of antibody on surface
 - Orientation of antibody (probably cannot be determined)
 - Blocking protein attached
 - Agglomeration state (pre-test)
 - Nanoparticle stability in test (non-specific binding to surfaces)
 - Change in agglomeration status in test (sample/matrix induced agglomeration)
2. Assay-specific uncertainties:
 - IL6 standard (purity, etc.)
 - Uncertainty in calibration response
 - Variation of instrument response (precision)
 - Temperature and humidity (flow)
 - Temperature and humidity (drying rate).
 - Wicking rate
 - Sample mixing and application time
 - Nanoparticle stability in test (non-specific binding to surfaces)
 - Change in agglomeration status in test (sample/matrix induced agglomeration)
 - Amount of nanoparticle-conjugates applied to test
 - Integration of the peak

As the FM3 and FM4 particles did not work very well in the lateral flow assays (problems with dye leaking and particle stability during bioconjugation and when applied to the test strips), the commercial fluorescent particles YG100a and YG200 were used instead to assess the nanoparticle-antibody conjugate-specific and assay-specific uncertainties (besides the amount of dye loaded, which could not be assessed for the commercial particles).

Conclusions

Fluorescent nanomaterials can be used to develop easy-to-use techniques for measuring the number of molecules in a sample (i.e. by binding to them and being revealed under UV illumination). The project developed a validated protocol for the SI traceable determination of relative and absolute fluorescence quantum yield of the fluorescent nanomaterials in aqueous media and biological serum. Traceable spectroscopic methods were also developed and validated for determining the parameters affecting the signalling behaviour of fluorescent nanomaterials, such as the number of proteins adsorbed onto the nanomaterials in biological systems.

With these methods the project successfully achieved its objective. The protocol for the traceable determination of relative and absolute quantum yields has been published as a journal paper and made available to laboratories working in the field of quantum yield analysis.

3.5 Objective 5: Development of measurement techniques for biotechnology using fluorescent nanomaterials.

The aim of this work was to use the reference materials from objective 1 to measure the fluorescent properties of nanomaterials attached to antibodies in biotechnology procedures. More specifically, to develop measurement techniques for biotechnology using fluorescent nanomaterials.

Assay Design

To understand the factors critical for successful application of fluorescent nanomaterials in the selected immuno(assay) design multiple particles types and fluorescent dyes were assessed. Initial assay development was based on detection of IL6 in a wound fluid mimetic and further suitable assays were developed using the YG100, YG200 and FM3 particles.

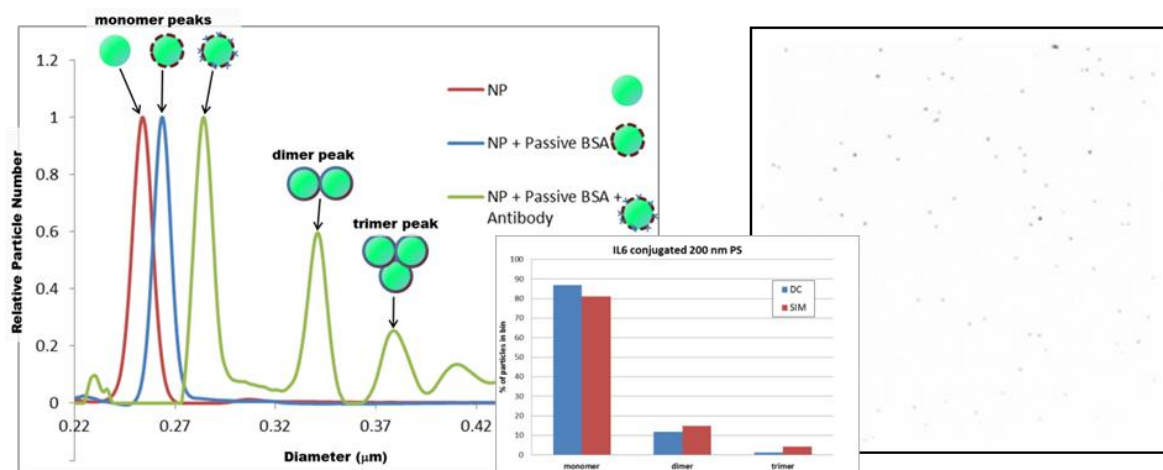
Unsuccessful attempts were made to generate antibody conjugated nanomaterials for FM4, and RM3 (quantum dot), as the antibody conjugated FM4 generated agglomerates with limited colloidal stability that could not be used in the developed lateral-flow device (LFD). RM3 also displayed poor recovery in size exclusion media during the washing steps of the conjugation reaction, and subsequently poor performance in the resulting LFD. In contrast, the IL6 assays developed using the YG100 and YG200 particles displayed suitable levels of assay performance, whereas FM3 could not be used to measure the analyte in the low pg/mL range. Despite this, FM3 was still used as a model system as it provided a direct link between assay uncertainty, and the optical and physical characterisation performed by BAM and other project partners, JRC and PTB. Finally, LFD assays using the fluorescent particles YG100, YG200 and FM3 were successfully developed and validated.

Preliminary assay development

Particle and protein analysis techniques were used to characterise the antibody-nanoparticle conjugates. This data was then compared with the signal generated by that conjugate in the LFD, to understand what properties of the nanoparticle influence the IL6 concentration estimate returned by the test. The following 6 particle and protein analysis techniques were used:

1. Dynamic light scattering (DLS): DLS was used to assess monomeric nanoparticle diameters to support Differential centrifugal sedimentation (DCS) calculations. DLS was also used to qualitatively assess the overall particle size of antibody conjugated particles; however this was only useful for samples that contained a small amount of contaminating oligomers (<20 %).
2. DCS was used to assess:
 - a. Size distribution – to quantitate the amount of contaminating oligomers.
 - b. The relative size of the antibody conjugated nanoparticle.
 - c. Protein (antibody) corona thickness on the nanoparticle.
3. Bicinchoninic acid (BCA) protein assay: The BCA assay was used to assess the amount of antibody and blocking protein attached to the nanoparticle.
4. Structured illumination microscopy (SIM): SIM was used to count the number of nanoparticle oligomers produced by different antibody conjugation reactions. The resolution of this method was limited to analysis of particles with a diameter of > 200 nm.
5. X-ray photoelectron spectroscopy (XPS): Attempts were made to use XPS to assess the thickness of the antibody corona layer on the nanoparticle, but unfortunately the assay could not be optimised for polystyrene nanomaterials.
6. Surface plasmon resonance (SPR): A competition assay was set up on a Biacore instrument to determine the amount and bio-activity of the antibody attached to each nanoparticle. This assay format provided activity data that was independent of the fluorescent properties of the particle. However, the assay did not have the sensitivity to differentiate small differences between the reference nanoparticle batches, which limited its application.

Due to the limitation of the other techniques to the project focussed on DCS, DLS and the BCA protein assay for nanoparticle bio-conjugate analysis. DCS analysis was found to be a useful tool for characterising the products of the antibody conjugation reaction to nanomaterials, allowing the quantitation of the particle size, degree of contaminating oligomers and an estimation of the amount of antibody attached (**Figure 17**). The use of DCS to measure antibody corona thickness (nm) also displayed a strong correlation with the amount of antibody present on the nanoparticle, as determined using the BCA protein assay. The project therefore concluded that in a qualitative manner DCS can be used to estimate the amount of antibody covalently bound (i.e. conjugated) to the nanoparticle.



A. DCS schematic.

B. SIM image of 200 nm particles.

Figure 17: A schematic highlighting the use of DCS and SIM to analyse antibody-particle conjugates. A: The DCS profiles of particles, antibody coated particles and contaminating oligomers. The DCS profile allows the analysis of particle size, contaminating oligomers and protein corona thickness due to separation based on size and density. B: A SIM image of particles embedded in a gel from which the number of contaminating particle oligomers in a conjugation reaction can be counted. Insert - shows the comparison between DCS and SIM techniques for assessing the ratio of contaminating oligomers present in antibody-particle conjugation reactions.

DCS proved to be a better method for characterising the products of antibody-nanoparticle conjugation reactions when compared to DLS size measurements. For all the fluorescent nanomaterials tested, a strong correlation was observed between the amount of contaminating oligomers present (as measured by DCS) and the resulting fluorescent response in the LFD. Multiple antibody conjugate batches were prepared for the FM3 and YG100 nanomaterials to represent industrial batch production and even small differences in the amounts of contaminating oligomer present ($\pm 10\%$), resulted in significant differences in the LFD fluorescence response. The presence of these contaminating oligomers represents a major uncertainty component for the use of fluorescent LFDs and may account for many of the batch-to-batch differences observed during industrial production of antibody coated nanomaterials. For many of the particles tested a strong correlation was also observed between the amount of antibody bound to the nanoparticle (as measured by the BCA assay and DCS) and the resulting fluorescent response in the LFD.

The optical properties of the fluorescent nanomaterials (FM1-4) as measured by project partner BAM were found to influence the analytical sensitivity of the resulting LFDs. Analysis was performed on the unmodified particles as the addition of an antibody corona to the nanoparticle was not found to significantly alter the spectroscopic properties of the particle. The following fluorescent properties of each particle were determined:

- Absorption-weighted emission intensities (AWEI): For the YG visible particles the YG200 200nm particles were significantly brighter than the YG100 100 nm particles. For the near infrared (NIR) particles significant differences existed between FM3 and FM4 that could not be explained.

- Fluorescent decay times: No significant differences were observed for the YG100 and YG200 particles; however FM3 displayed a significantly shorter decay time than FM4, which is in accordance with the AWEI and absolute QY data.
- Absolute quantum yields (Absolute QY): All the visible YG100 and YG200 particles displayed a greater Absolute QY, ~ 0.75 , when compared to the NIR particles which gave an Absolute QY range of 0.17 – 0.47. Again significant differences were observed between FM3 and FM4.

This spectroscopic characterisation of the fluorescent nanomaterials provided the project with evidence of the different analytical sensitivities observed when incorporated into a LFD. In general, the project concluded that YG particles displayed AWEIs when compared to the NIR particles. Furthermore, DCS analysis can be used by assay manufacturers to compare differences in batch production of antibody conjugated nanomaterials, or to understand why a specific batch has failed quality control. The project also showed that (based on spectroscopic data) the selection of the most appropriate fluorescent dye for nanoparticle doping plays a critical role in defining the measurement parameters of the resulting immunoassay).

Assay optimisation and validation

The assessment of the uncertainty in the IL6 LFD was conducted with the aim to identify uncertainty components that could be minimised through improved measurement practice. The measurand was defined as the amount of IL6 in picograms in 1 mL of human serum, as determined using a lateral flow test with YG100 fluorescent particles and measured using an ESE-Quant reader. The key uncertainty components that were investigated by the project were associated with:

- Performance of the fluorescent reader instrumentation
- Reproducibility of the antibody-nanoparticle conjugation reaction
- Environmental conditions
- Reproducibility associated with the generation of the analyte calibration response

From the results, it could be seen that the uncertainty associated with batch-to-batch production of antibody conjugated nanomaterials was typically $\sim 10\%$ relative standard deviation. This was significant; however it could be minimised through the use of quality controlled (QC) materials and adjustment of the calibration response, and was therefore omitted from the expanded uncertainty budget, by the project. For IL6 quantitation in serum the expanded ($k=2$) uncertainty budget derived was 1100 ± 108.2 pg/mL. The 10% relative uncertainty was consistent across the required measurement range for IL6 detection and is within the limits set by the majority of assay validation guidelines.

In summary of the results, for immunoassay developers using fluorescence (nanomaterials) for detection, the following should be considered to reduce the overall uncertainty:

- Instrument calibration using a fluorescent standard. Environmental conditions influence the instrument response (1000 ± 17 pg/mL of IL6 per $\Delta^\circ\text{C}$), therefore calibration should ideally be performed at multiple time points during the day, or if the instrument is moved to another location. The latter is significant for portable tests that are often used in point-of-care (POC) testing.
- Preparation of calibrants and QC material at a larger scale, preferably at the working concentration range, so as to reduce the uncertainty associated with liquid handling.
- The use of automated wait sequences to control the assay development time, these should be incorporated into the measurement protocol, ideally integrated into the fluorescent reader software. The project observed a strong correlation between fluorescent response and assay development time, requiring the use of a defined assay development time to reduce this uncertainty component.

Conclusions

Fluorescent nanomaterials can be attached to antibodies that bind with specific target molecules (such as those produced by tumour cells), to indicate the presence, and importantly, the quantity of the target molecule in a sample. To better understand how the properties of antibody-bound nanoparticles influence their



performance in biotechnology procedures, the fluorescent nanoparticles produced in objective 1 were integrated into an Interleukin 6 (IL-6) antibody procedure. This procedure was then used to successfully demonstrate the use of disc centrifugation for determining the relative quantities of agglomerated antibody conjugated nanoparticle.

The objective was successfully achieved, as suitable levels of accuracy were obtained for the procedure to be appropriate for validation of measurements in biotechnology laboratory processes. In addition, the uncertainty data generated by this research highlighted ways that manufacturers of biotechnology procedures can improve the performance of quantitative lateral flow assays.

4 Actual and potential impact

Dissemination of results

To promote the uptake of the reference materials and techniques developed, project results were shared broadly with scientific and industrial end-users. 12 papers were published in international scientific journals (listed in the next section). The project was also publicised with an article '[Nanotechnology: The Big Challenge Behind the Characterization of the Small](#)', published on both the UK Nano Knowledge Transfer Network website, and the Drug Discovery & Development website (the latter reaches approximately 35-50k readers from the pharmaceutical industry, academia, manufacturers of instruments and nanomaterials). 47 presentations were given at international symposiums, including Nanosafety 2013 and 2014. The research consortium has also been active in organising and participating in workshop and training events with the end user community, including a Nanoparticle Workshop in April 2015, with approximately 100 end users, predominantly from higher education and public research organisations.

Impact on standardisation

The project has had significant impact on standards for assessing nanoparticle properties and safety. Examples include: LGC's contribution to the production of BSI guidelines (PAS 139) on the detection and characterisation of nanomaterials in biological samples (related to the international standard ISO/TC 229). BAM's contribution to the production of a standard guide for fluorescence measurements [ASTM E2719-09(2014)]. JRC's input into the draft documentary standard ISO 22412 "Particle size analysis-dynamic light scattering" (related to ISO/TC 24), and their input into vocabulary/terminology for ISO/TC 229 documents on nanotechnologies [e.g. quantum phenomena in nanotechnology (DTS 80004-12) and Plain Language Guide to vocabulary (ISO/TR 18401)].

Early impact on industry

Project outputs have already been shared with industry, and have been used to improve products and services: Nanomaterials from microParticles GmbH, PlasmaChem, Colorobbia and CAN were tested during work for objective 1. Results from testing were fed back to these companies, particularly on the stability, homogeneity, polydispersity and other important production quality parameters. This feedback, and knowledge acquired during the project, will be used to manufacture higher-performance nanomaterials for academic and industrial users, and is being used in the current EURAMET project [Innanopart](#) to develop new methods to characterise nanomaterial properties for industry. Insights developed from the production of reference nanomaterials were also shared with partner National Measurement Institutes, and guidance on the in-house preparation of quality control nanomaterials has been shared with reference material producers.

Malvern Instruments Ltd (a manufacturer of laboratory analytical equipment) has adopted the method developed in objective 2 for evaluating the performance of nanoparticle tracking analysis (NTA), to measure nanoparticle concentrations and sizes. Malvern's NTA output in terms of number based concentration offers great potential to assess if materials meet the European Commission's definition of a nanoparticle, necessary for determining whether or not the material will be subject to European safety regulations. Additionally, feedback was provided to Malvern Instruments on recommended improvements to their NTA software. The software has since been upgraded, and now allows users to study individual nanoparticle populations, and to resolve them within high serum concentrations, as required by nanotoxicology tests. In recognition of the project's contributions, Malvern Instruments have published a [case study](#) on their website describing the benefits of Nano ChOp results for their business. Following from the successful contributions to Malvern Instruments, CPS Instruments (another manufacturer of laboratory equipment) has entered into discussion with Nano ChOp researchers to explore ways to improve their centrifugal liquid sedimentation instrumentation software, and their related calibration approaches for nanomaterial characterisation.

As part of objective 3, the project evaluated equipment from Postnova Analytics (a developer of nanoparticle detection systems). Feedback was given to Postnova on their field flow fractionation detection modules, and as a consequence the company has upgraded a number of their products, which will enable academic and industrial users to develop faster and simpler nanoparticle detection and characterisation processes.

Potential future impact on industry

The reference nanomaterials and the measurement techniques developed by this project are the first of their kind, and will lead to a better understanding of the properties of current and future nanoparticles. They will play a key role in ensuring the safe use of nanomaterials; results will be used by nano-biotechnology and nano-medicine organisations to validate their protocols, and to perform toxicology studies and risk assessments. Regulatory bodies and legislators will benefit from a clearer understanding of the effects of nanomaterials on health, and will have a foundation upon which they can develop policies and guidelines. The important first step made by this project in the understanding of the properties of antibody-bound nanoparticles has laid the foundations for the increased use of nanoparticles in medicine and healthcare.

The achievements of this project have established avenues for additional scientific research, further developed in the EURAMET projects [HLT02 MetVes](#) (detection of microvesicles in body fluids) and [14IND12 Innanopart](#) (measuring nanoparticle concentrations). The development of multi-method approaches for characterising nanoparticle properties has also complement the work of [NanoDefine](#), a current EU project implementing a standardised EC definition of a nanomaterial. Ultimately, the results of this project will enable European nanotechnology researchers and industry to develop new, safe, higher-performance products and processes.

5 Website address and contact details

JRP website address: <http://nanochop.lgcgroup.com/>

JRP-Coordinator: Dr. Heidi Goenaga-Infante, LGC

E-mail: Heidi.Goenaga-Infante@LGCGroup.com

6 List of publications

- [1]. C. Würth, M. Grabolle, J. Pauli, M. Spieles, U. Resch-Genger, Relative and absolute determination of fluorescence quantum yields of transparent samples, *Nature Protocols*, July 2013, Vol. 8, No. 8, pp. 1535-1550.
- [2]. S. J. Rödiger, C. Liebsch, C. Schmidt, W. Lehmann, U. Resch-Genger, U. Schedler, P. Schierack, Nucleic acid detection based on the use of microbeads: a review, *Microchimica Acta*, April 2014 (online), DOI 10.1007/s00604-014-1243-4.
- [3]. M. Müller, M. Kaiser, G.M. Stachowski, N. Gaponik, U. Resch-Genger, A. Eychmüller, Photoluminescence Quantum Yield and Matrix-Induced Luminescence Enhancement of Colloidal Quantum Dots Embedded in Ionic Crystals, *Chem. Mater.*, April 2014, Vol. 26, No. 10, pp. 3231–3237.
- [4]. K. Hoffmann, T. Behnke, M. Grabolle, U. Resch-Genger, Nanoparticle-encapsulated Vis- and NIR-emissive Fluorophores with Different Fluorescence Decay Kinetics for Lifetime Multiplexing, *Analytical and Bioanalytical Chemistry*, May 2014, 406 (14): 3315-22.
- [5]. M. Pálmai, R. Szalay, D. Bartczak, Z. Varga, L. Naszályi Nagy, C. Gollwitzer, M. Krumrey, H. Goenaga-Infante, Total synthesis of isotopically enriched Si-29 silica NPs as potential spikes for isotope dilution quantification of natural silica NPs, *Journal of Colloid and Interface Science*, 2015, 445, pp 161-165.
- [6]. D. Bartczak, P. Vincent, H. Goenaga-Infante, Determination of size- and number-based concentration of silica nanomaterials in complex biological matrix, *Analytical Chemistry*, 2015, 87 (11), pp 5482–5485.
- [7]. C. Würth, D. Geißler, T. Behnke, M. Kaiser, U. Resch-Genger, Critical review of the determination of photoluminescence quantum yields of luminescent reporters, *Analytical and Bioanalytical Chemistry*, 2015, 407 (1), 59-78, doi:10.1007/s00216-014-8130-z.
- [8]. C. Würth, D. Geißler, U. Resch-Genger, Quantification of Anisotropy-Related Uncertainties in Relative Photoluminescence Quantum Yield Measurements of Nanomaterials – Semiconductor Quantum Dots and Rods, *Z. Phys. Chem.* 2015, 229 (1–2), 153-165, doi:10.1515/zpch-2014-0626.

- [9]. C. Würth and U. Resch-Genger, Determination of Photoluminescence Quantum Yields of Scattering Media with an Integrating Sphere: Direct and Indirect Illumination, *Appl Spectrosc.* 2015, 69 (6), 749-59, doi: 10.1366/14-07679.
- [10]. Sikora, D Bartczak, D. Geißler, V. Kestens, G. Roebben, Y. Ramaye, Z. Varga, M. Palmi, A. G. Shard, H. Goenaga-Infante, and C. Minelli. A systematic comparison of different techniques to determine the zeta potential of silica nanomaterials in biological medium, *Anal. Methods*, 2015, 7, pp 9835-9843.
- [11]. G. Roebben, et al., Reference materials and representative test materials to develop nanoparticle characterisation methods: The NanoChop project case. *Frontiers in Chemistry*, 2015, doi: 10.3389/fchem.2015.00056 (open access)
- [12]. C. Gollwitzer, D. Bartczak, H. Goenaga-Infante, V. Kestens, M. Krumrey, C. Minelli, M. Palmi, Y. Ramaye, G. Roebben, A. Sikora and Z. Varga, 2016. A comparison of techniques for size measurement of nanoparticles in cell culture medium. *Anal. Methods* 2016, 8, pp 5272-5282.